CHAPTER 4

Development and characterisation of an anti-Basigin chimeric antibody, as a putative anti-malarial therapeutic

4.1 Summary and Aims

The interaction between *P. falciparum* RH5 and BSG has been shown to be essential and universally required for erythrocyte invasion (Crosnier *et al.*, 2011). Antibodies against either RH5 or BSG could potently inhibit merozoite invasion in parasite culture, in all *P. falciparum* strains that have been examined (Crosnier *et al.*, 2011; Douglas *et al.*, 2011; Bustamante *et al.*, 2013). Therefore, the blockade of RH5-BSG interaction can be exploited for therapeutic purposes, for the treatment of *P. falciparum* infected individuals.

Most of the work described in this Chapter, was aimed at the development of a humanised or chimeric anti-BSG antibody as a potential anti-malarial therapeutic. By employing the versatile plasmid system which was developed in Chapter 3, two anti-BSG antibodies, MEM-M6/4 and MEM-M6/8 (gift from Prof. Vaclav Horejsi; Koch *et al.*, 1999), were humanised (hu) by Complementarity Determining Region (CDR) grafting, and expressed recombinantly. Despite preserving their ability to bind BSG *in vitro*, huMEM-M6/4 and huMEM-M6/8 could not block erythrocyte invasion when tested in *P. falciparum* erythrocyte invasion assays. This result was found to be due to the low affinity for BSG, of both mouse and humanised antibodies.

To obtain an anti-BSG monoclonal that would be effective for this application, I immunised mice to select several new hybridoma lines secreting anti-BSG monoclonal antibodies. An anti-BSG antibody that I named m6D9, was secreted by one of the generated hybridoma clones, and was prioritised for further study since it demonstrated very high efficacy in blocking the RH5-BSG interaction *in vitro*, and in preventing erythrocyte invasion in *P. falciparum* parasite culture. While attempts to fully humanise m6D9 were unsuccessful, a chimerised antibody, ch6D9 retained its high affinity for BSG and demonstrated high potency in blocking erythrocyte invasion in all parasite lines tested. Furthermore, ch6D9 displayed reduced binding to FcγRIIA and C1q *in vitro*, suggesting that this antibody may have reduced ability to trigger antibody effector functions.

In a parallel approach, two anti-RH5 monoclonals (2AC7 and 9AD4; Douglas *et al.*, 2013) were successfully chimerised. Both ch2AC7 and ch9AD4 preserved their high affinity for RH5 and inhibited erythrocyte invasion in parasite culture, but with much higher IC_{50} as compared to ch6D9. In an attempt to increase the potency and

selectivity of the antibodies, the variable regions of ch2AC7 and ch6D9 were combined in an anti-RH5 and anti-BSG bi-specific antibody: 2AC7-6D9 DVD-Ig. 2AC7-6D9 DVD-Ig was capable of simultaneous binding to RH5 and BSG, but its affinity for BSG decreased in comparison to ch6D9. When tested in a *P. falciparum* growth inhibition assay, 2AC7-6D9 DVD-Ig was more effective than ch2AC7, but less than ch6D9 in blocking erythrocyte invasion. These results suggest that the anti-BSG ch6D9 has higher potency in inhibiting erythrocyte invasion, than the anti-RH5 ch2AC7 or the bi-specific anti-RH5/BSG 2AC7-6D9 DVD-Ig.

4.2 Introduction

4.2.1 Surface Plasmon Resonance-A valuable tool for measuring the affinity of antibodies and other molecules to their targets

One of the key parameters of antibodies is their affinities for their target. In this Chapter as well as in Chapter 5, I used Surface Plasmon Resonance (SPR) to biophysically characterise the interaction between two proteins; and in this Chapter, between an antibody and its antigen. While increasingly becoming a mainstream research tool, a brief description of this method and its applications is perhaps warranted. SPR optical biosensors exploit the evanescent wave phenomenon to derive information about the physical interactions between an immobilised ligand and a soluble analyte, in real time (Fig 4.1A). When plane-polarised light is shone through a prism - at an angle that leads to total internal reflection - on a conducting film placed at the interface between two media of different refractive index, surface plasmons (coherent oscillating electrons) are generated (Schasfoort and Tudos, 2008). Plasmon excitation is caused by resonance conditions that are established when the frequency of the photons constituting the incident light, matches the natural oscillation frequency of surface electrons. The energy transfer from incident photons to the surface electrons leads to a drop in the intensity of the reflected light at a characteristic angle known as the SPR angle. The SPR angle is dependent upon the relative refractive indices between a glass slide and the region close to the interface, which, in the case of an SPR machine used for protein interaction research, is a small flow cell contained within a disposable chip. The changes in refractive index within the flow cell caused by the accumulation of mass (e.g. proteins) leads to a change in the SPR angle that can be measured in real time and provides information

A.

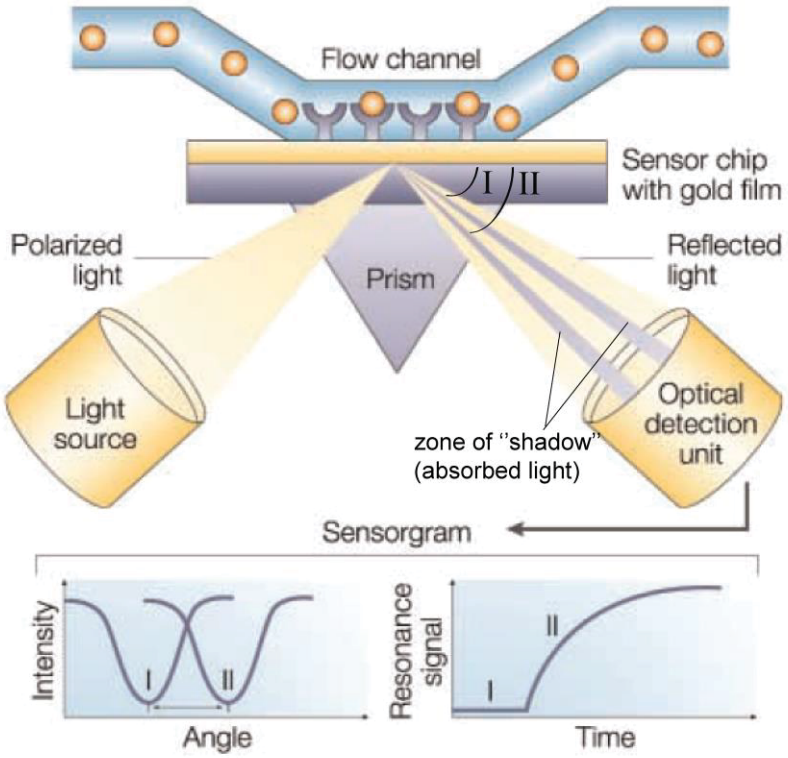
Flow channel
Sensor chip
with gold film
I II
Polarized
light
Prism
Reflected
light
Light
source
zone of "shadow"
(absorbed light)
Optical
detection
unit
Sensorgram
Intensity
I
II
Angle
Resonance
signal
I
II
Time

B.

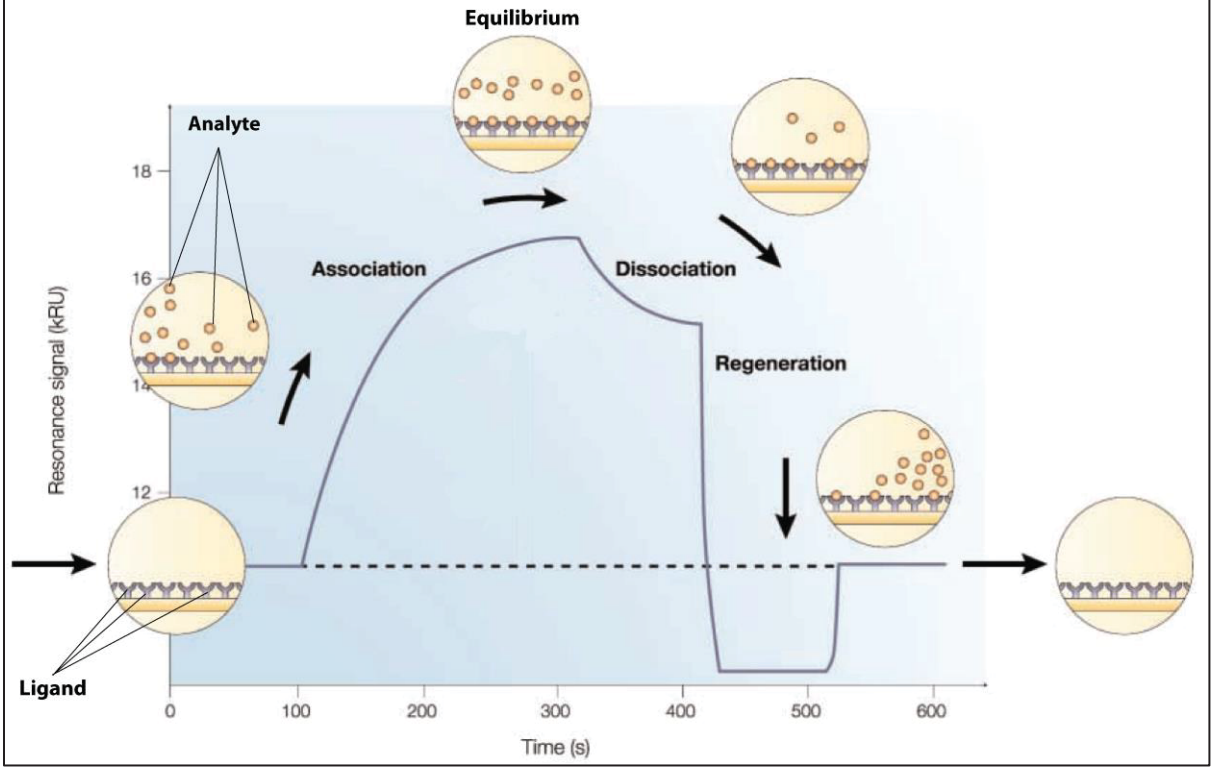
Equilibrium
Analyte
18
16
14
12
Association
Dissociation
Regeneration
Resonance signal (kRU)
Ligand
0
100
200
300
400
500
600
Time (s)

Figure 4.1 Surface Plasmon Resonance.

A. A typical biosensor setup. Polarized light is shone through a prism on a sensor chip, under conditions of total internal reflection. The absorbance of photon energy by surface electrons results in the loss of intensity of the reflected light at a particular reflection angle (SPR angle; angle I). The binding of molecules on a thin layer in the close vicinity of the gold surface on the chip, results in changes in the refractive index which in turn alters the SPR angle (angle II). These changes in resonance angle can be monitored in real time, and the resonance signal can be plotted against time (graph on the bottom right).

B. A typical sensogram obtained during a Surface Plasmon Resonance experiment. The ligand is immobilised in a flow cell by using appropriate chemistry (t=0). At t=100s, the analyte is injected into the flow cell where the ligand is immobilised. As the analyte binds to the ligand, the refractive index adjacent to the sensor surface increases, leading to an increase in the resonance signal. The association rate constant (k_a) can be determined by mathematical analysis of this part of the binding curve (Cooper, 2002). Continuation of analyte flow over the ligand will lead to equilibrium, where the association and dissociation rates are equal. The response level at equilibrium is related to the concentration of active analyte in the sample. At t = 320s, the analyte injection is ceased and the receptor–analyte complex is left to dissociate. Analysis of these data gives the dissociation rate constant (k_d) for the interaction. Many biological interactions have extensive half-lives, and therefore a pulse of a regeneration solution (normally high salt or low pH) is required (t = 420s) to disrupt binding and regenerate the free ligand. The entire binding cycle is normally repeated several times with a concentration series of analyte to generate a reliable data set which can then be used for global fitting to an appropriate binding algorithm. The affinity of the interaction can be calculated from the ratio of the rate constants ($K_D = k_d / k_a$) or by a linear or nonlinear fitting of the response at equilibrium ($R_{maximum}$) at varying concentrations of analyte. Pictures adapted and modified from Cooper, 2002

on the affinity and kinetics of a particular interaction (Fig 4.1) (Cooper, 2002; Schasfoort and Tudos, 2008).

Biacore technology, which is the one that was employed for the purposes of my experiments, utilizes sensor chips containing a thin film of gold built on a glass surface over which a solution containing the sample is passed (Fig. 4.1). Normally, a Biacore experiment starts by immobilising the ligand on the chip surface by using the appropriate coupling chemistry. The analyte is then injected over the immobilised ligand and the changes in SPR angle are monitored in real time and obtained in the form of sensorgrams (Fig. 4.1B). By adjusting the flow rate and duration of analyte injection, and by using the appropriate mathematical analysis, binding affinities and kinetics can be determined (Cooper, 2002).

4.2.2 Antibody humanisation approaches

Monoclonal antibodies (mAbs) have been an invaluable tool towards the treatment of serious diseases affecting mankind, like cancer, autoimmunity and viral infections (Reichert *et al.*, 2005; Carter, 2006). The utility of mAbs as therapeutics was recognised shortly after the introduction of hybridoma technology by Köhler and Milstein in 1975 (Köhler and Milstein, 1975). Their high affinity and exquisite specificity has rapidly put mAbs to a central position in the class of biological drugs (Beck *et al.*, 2010). However, it was soon realised that mAbs derived from hybridoma technology, are strongly immunogenic when injected in humans. Several studies reported that human-anti-mouse antibody (HAMA) responses were apparent in about 50% of patients after a single injection of murine mAbs, and in more than 90% of patients following two or three repeated injections (Qu *et al.*, 2005). A more extensive survey study, covering the period between January 1984 to December 2003, reported that 84% of murine mAbs surveyed, elicited marked HAMA reactions (more than 15% of the patients developed HAMA), 7% stimulated tolerable HAMA responses (2-15% of the patients developed HAMA), while 9% had negligible HAMA (<2% of the patients developed HAMA) (Hwang and Foote, 2005). As a result, murine mAbs are cleared rapidly in the human body and therefore, they have poor pharmacokinetics with short half-lives. Additionally, mouse mAbs are unable to trigger antibody effector functions such as complement activation or T cell stimulation, when injected into patients (Qu *et al.*, 2005; Tsurushita *et al.*, 2005).

The first attempts to reduce mAb immunogenicity led to the development of mouse-human chimeric mAbs which were generated simply by replacing the constant heavy and light chains of the mouse antibody under investigation, with the respective sequences found in human antibodies (Morrison *et al.*, 1984). The advantage of this approach is that the antibody specificity and affinity is retained because the entire variable regions are transplanted, without altering their amino acid composition which might affect the binding to the antigen. Approximately 60-70% of chimeric antibody (chAb) sequence is of human origin (Gonzales *et al.*, 2005; Qu *et al.*, 2005). Nevertheless, chAbs are still significantly immunogenic since 40% of the chAbs tested between January 1984 and December 2003 elicited marked anti-antibody responses (see above) (Hwang and Foote, 2005).

Since those first trials, more sophisticated approaches have been devised to reduce the murine amino acid content of therapeutic antibodies. In the mid-1980s Dr. Greg Winter and colleagues at the MRC Cambridge, introduced the Complimentarity Determining Region (CDR) grafting technology (Jones *et al.*, 1986; Riechmann *et al.*, 1988). This approach exploits the fine structure of immunoglobulin variable regions which consists of four framework regions (FRs) separated by three CDRs (section 1.2). The antigen-binding specificity of a murine antibody is transferred to a human antibody by replacing the CDR loops (Jones *et al.*, 1986; Riechmann *et al.*, 1988; Gorman and Clark, 1990; Lo, 2004).

In the CDR grafting approach, it is of great importance that key residues in murine FRs are identified and incorporated into the humanised antibody. Nevertheless, it is a common phenomenon that the affinity of a humanised antibody for its antigen, is greatly reduced as compared to the parental mouse one (Lo, 2004; Almagro and Fransson, 2008). The decrease in antibody affinity is likely to be due to incompatibilities between human FRs and murine CDRs. Antibody affinity can potentially be restored by mutating certain amino acids in the FRs of the humanised antibody back to those found at the same position in the murine parental antibody (Lo, 2004; Almagro and Fransson, 2008). The identification of the residues to be mutated is not trivial, and requires expertise in three dimensional modelling (Lo, 2004; Almagro and Fransson, 2008).

With regards to immunogenicity, the non-human sequence composition of a CDR-grafted antibody is typically only 5–10% compared to about 30% for a chimeric

antibody, and it was predicted to be minimally immunogenic (Lo, 2004; Gonzales *et al.*, 2005). Indeed, humanised antibodies were well tolerated, and several clinical trials reported undetectable or minimal anti-immunoglobulin responses (Sharkey *et al.*, 1995; Cobleigh *et al.*, 1999; Kalunian *et al.*, 2002; Crombet *et al.*, 2004). Another study, however, reported that a considerable amount of patients developed anti-antibody responses (Herold *et al.*, 2005), indicative that there was still space for improvement in terms of the "extent" of humanisation.

Padlan and colleagues further refined the antigen binding site within the CDRs: they identified that only 20–33% of the CDR residues participate in antigen-binding (Padlan, 1994), and these residues have been designated as specificity determining residues (SDRs) (Padlan *et al.*, 1995). Tamura and colleagues were the first to successfully humanise an antibody (the CC49 anti-TAG72 mAb) by grafting only the SDRs of the murine antibody into the human antibody FRs (Tamura *et al.*, 2000). This antibody showed reduced immunogenicity in comparison to the CDR grafted CC49 (Tamura *et al.*, 2000). However, similar to humanisation by CDR grafting, the SDR grafting approach entails the risk of significant loss of antigen-binding affinity (Kashmiri *et al.*, 2005; Kim and Hong, 2012).

Finally, antibodies having their entire amino acid content of human origin have been developed by using transgenic animals. Transgenic mice have been genetically engineered, and the genes encoding for the human antibody repertoire have been inserted into the mouse genome, functionally replacing the endogenous mouse loci (Lonberg, 2005; Jakobovits *et al.*, 2007). Therefore, immunisation of these mouse models with the antigen of interest results in the generation of human monoclonal antibodies. A number of different transgenic mouse platforms for antibody discovery exist, but the wide adoption of this technology has been hampered by complications with regards to the commercial rights (Moran, 2013).

4.2.3 Combination therapies and the value of bi-specific agents

Combination therapy is a widely acknowledged tactic to confront a range of diseases. By definition, in combination therapy two or more drugs are used together to treat a single disease. Simultaneous blockade of more than one molecules implicated in the same disease pathway is likely to provide better clinical efficacy (Wu *et al.*, 2007). Another major benefit of combination therapy is the reduced risk of

drug resistance development: it is less likely for the disease factor to simultaneously develop resistance to multiple defences, than to one alone. Conditions that are currently being treated with combination therapy include, tuberculosis (Diacon *et al.*, 2012), HIV (Bartlett, 1996; Hirsch *et al.*, 2003) and malaria (Miller *et al.*, 2013). Specifically for malaria, artemisinin-based combination therapies, comprise the first line of defence (Miller *et al.*, 2013).

Combination therapies have also been considered in the case of antibodies. Importantly, in June 2012 an antibody based combination therapy has been approved by FDA, for the treatment of patients with HER2-positive metastatic breast cancer who have not received prior anti-HER2 therapy or chemotherapy for metastatic disease (Blumenthal *et al.*, 2013). However, the co-administration of two or more antibodies to patients, requires complex pharmacokinetics and safety studies which complicates their routine use in clinic (Wu *et al.*, 2007). To avoid this problem, antibody based agents with multiple specificities have been developed. The first attempts to develop bi-specific antibodies were based on a “mix and match” approach where two hybridoma lines producing antibodies of the desired specificities, were fused to form a quadroma (Milstein and Cuello, 1983). Although the resulting hybrid did produce bi-specific antibodies the yields were very low, and only a small fraction of the secreted antibodies had dual specificity.

With the advent of recombinant DNA technology, more sophisticated approaches have been devised to force hetero-dimerization of two antibody arms of different specificity, and thereby resulting in a bi-specific antibody (Davis *et al.*, 2010; Schaefer *et al.*, 2011; Wranik *et al.*, 2012; Labrijn *et al.*, 2013). Other approaches utilize antibody fragments which are fused together in a multi-specific agent (Holliger and Hudson, 2005; Morrison, 2007; Chames and Baty, 2009). Because of their small size, such agents are very versatile and especially when used against solid tumors they demonstrate high penetration and uniform bio-distribution (Holliger and Hudson, 2005; Chames and Baty, 2009). However, most of these engineered antibody fragments have poor pharmacokinetics, because they lack the antibody Fc region which is responsible for antibody recycling. Wu and colleagues described a new methodology to produce full-sized bi-specific antibody molecules, which they named dual–variable domain immunoglobulin or DVD-Ig (Wu *et al.*, 2007). Each heavy and light chain contains two tandem variable domains, joined between each other by a

linker peptide (Fig. 4.19A). As a result each arm of the derived tetravalent molecule is capable of binding to two different antigens at the same time.

4.3 Results

4.3.1 Characterisation of MEM-M6/4 and MEM-M6/8 anti-BSG monoclonal antibodies

In Chapter 3, I described the establishment of a plasmid system which enables the recombinant expression of engineered antibodies. This system was a necessary tool for the subsequent development of an anti-BSG humanised mAb. Nevertheless, the development of a humanised anti-BSG antibody by CDR grafting, also required the availability of an anti-BSG mAb raised in animals, to serve as CDR donor. For this purpose, I would ideally choose one of the five anti-BSG antibodies (MEM-M6/6, MEM-M6/1, TRA-1-85, 8J251 and P2C2-1-D11) which were previously tested in our laboratory and demonstrated high efficacy in blocking erythrocyte invasion in parasite culture (Crosnier *et al.*, 2011; Bustamante L., unpublished; Theron M., unpublished). However, all of these antibodies were commercially available and therefore, I had no access to the respective hybridoma lines producing them, from where I would be able to amplify and sequence the antibody variable regions (see below). Therefore, we sought such hybridoma lines from the literature and we got access to two of them, namely MEM-M6/4 and MEM-M6/8 (Koch *et al.*, 1999). Both these lines originated from the same panel of mouse hybridoma lines as MEM-M6/6 and MEM-M6/1, two of the five high efficacy mAbs previously tested in our laboratory (see above). Considering that all five anti-BSG antibodies tested in earlier experiments were able to block erythrocyte invasion, it was expected that MEM-M6/4 and MEM-M6/8 would also be able to do so.

To biochemically characterise MEM-M6/4 and MEM-M6/8 mAbs, the respective hybridoma lines were grown in culture, and MEM-M6/4 and MEM-M6/8 mAbs were purified from tissue culture supernatant by affinity chromatography on a protein G column (Fig. 4.2A). To ensure that antibody heavy and light chains were assembled and secreted as a functional antibody, the purified antibodies were analysed by denaturing or native SDS-PAGE (Fig. 4.2B). Antibody heavy and light chains were stoichiometrically balanced in their expression level and capable of association (Fig. 4.2B). Unpurified antibodies from tissue culture supernatant as well as protein G

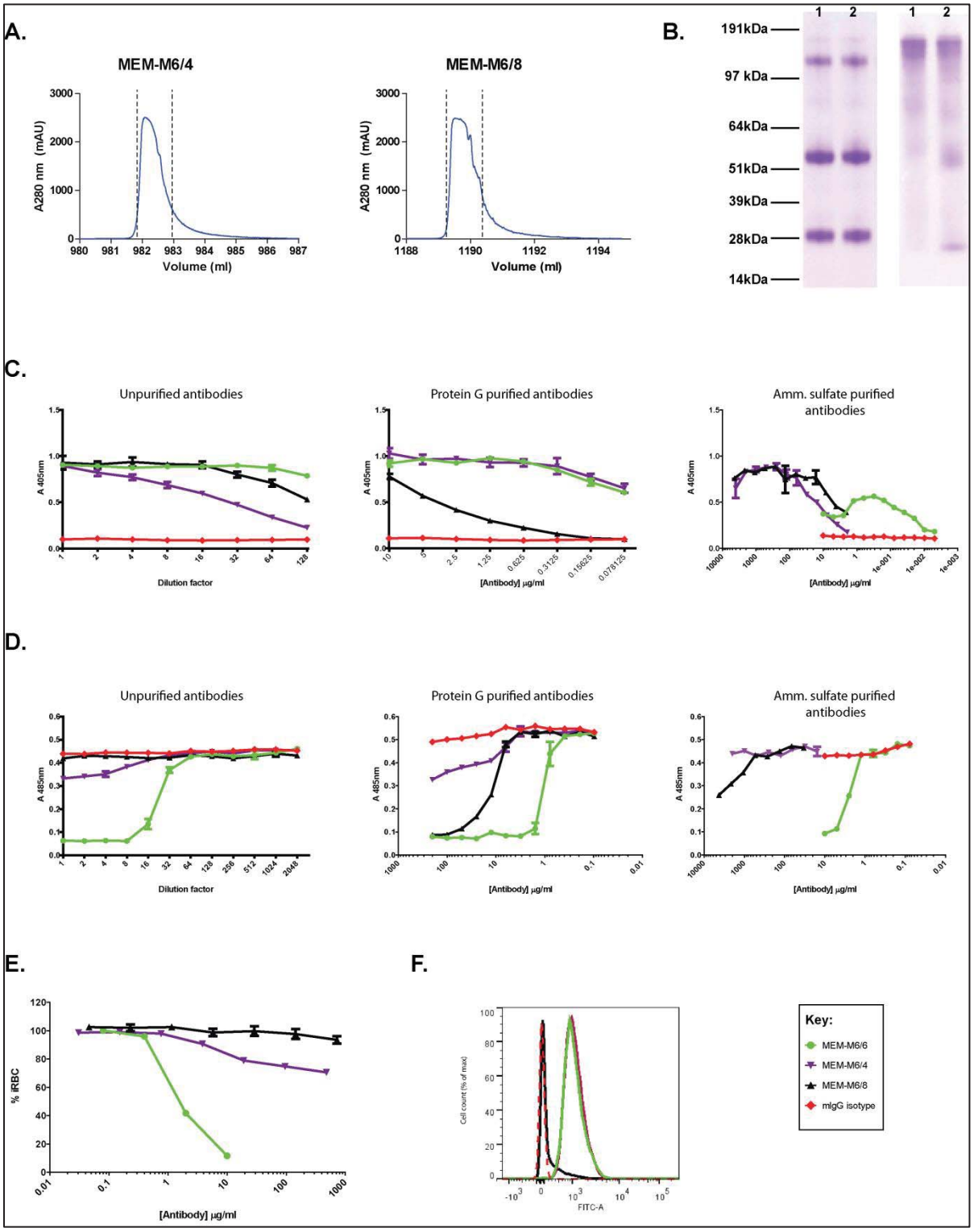
A.
MEM-M6/4
MEM-M6/8
A280 nm (mAU)
Volume (ml)
B.
191kDa
97 kDa
64kDa
51kDa
39kDa
28kDa
14kDa
1 2 1 2
C.
Unpurified antibodies
Protein G purified antibodies
Amm. sulfate purified antibodies
A 405nm
Dilution factor
[Antibody] µg/ml
D.
Unpurified antibodies
Protein G purified antibodies
Amm. sulfate purified antibodies
A 485nm
Dilution factor
[Antibody] µg/ml
E.
% iRBC
[Antibody] µg/ml
F.
Cell count (% of max)
FITC-A
Key:
MEM-M6/6
MEM-M6/4
MEM-M6/8
mIgG isotype

Figure 4.2 Characterisation of MEM-M6/4 and MEM-M6/8 anti-BSG, mouse monoclonal antibodies.

A. MEM-M6/4 and MEM-MEM-6/8 were affinity purified from tissue culture supernatant on protein G column. The eluate in each experiment was monitored at 280 nm in real-time and the peak fractions containing recombinant antibodies (between dashed lines) were pooled.

B. Protein G purified MEM-M6/4 (lane 1) and MEM-MEM-6/8 (lane 2) were analysed by SDS-PAGE under reducing (left) or non-reducing (right) conditions, and visualized by Coomassie brilliant blue. Under reducing conditions (left), two bands were observed for each antibody, at 55 and 28 kDa, representing antibody heavy and light chain respectively. The band at about 100kDa likely represents non-completely reduced antibody molecules. Under native conditions (right), most of the signal was concentrated to a single band at 150kDa, which is characteristic of fully assembled antibody.

C. Unpurified (left), protein G purified (middle) or ammonium sulfate purified (right) MEM-M6/4 and MEM-M6/8 were able to bind BSG, in an ELISA assay. BSG-BLH from tissue culture supernatant was immobilised on a streptavidin-coated plate at concentrations sufficient for complete saturation of the available binding surface, followed by incubation with a dilution series of each antibody. The binding of each antibody to BSG was determined by using an anti-mIgG secondary, conjugated with alkaline phosphatase.

D. The inhibitory effect of unpurified (left), protein G purified (middle) or ammonium sulfate purified (right) MEM-M6/4 and MEM-M6/8 on RH5-BSG interaction, as assessed by AVEXIS (for details see text). RH5 was used as bait, and pentameric BSG as prey. Pentameric BSG prey was pre-incubated with a dilution series of each antibody prior to probing RH5-BLH which was pre-immobilised on a streptavidin-coated plate.

E. Protein G purified MEM-M6/4 and MEM-M6/8 antibodies did not block erythrocyte invasion in parasite culture. Synchonised schizonts were incubated overnight with a dilution series of each antibody, before fixed and stained with SYBR Green I. The graph shows the percentage of infected red blood cells (iRBC) as a function of antibody concentration.

F. Binding of protein G purified MEM-M6/4 and MEM-M6/8 to human erythrocytes. Red blood cells were incubated with each antibody, followed by incubation with a FITC-conjugated anti-mIgG secondary and analysis by flow cytometry. The histogram shows the normalised cell count as a function fluorescence intensity at the FITC emission wavelength.

Data in *C*, *D* and *E* are shown as mean ± standard error; n=3. In all experiments the anti-BSG antibody MEM-M6/6 was used as positive control, and a mIgG isotype as negative. Where tissue culture supernatant was used for experiments, the starting concentration for MEM-M6/6 or mIgG isotype control was 10µg/ml.

purified MEM-M6/4 or MEM-M6/8, were then tested for binding to BSG by ELISA. Both MEM-M6/4 and MEM-M6/8 demonstrated binding to BSG (Fig. 4.2C). These data suggest that MEM-M6/4 and MEM-M6/8 were secreted from hybridoma lines in a biochemically active form, and were capable of binding to BSG *in vitro*.

4.3.2 MEM-M6/4 and MEM-M6/8 inhibit the RH5-BSG interaction *in vitro,* in AVEXIS assay, when used at high concentrations

To test whether MEM-M6/4 and MEM-M6/8 were able to block the RH5-BSG interaction *in vitro,* I employed the AVEXIS assay (Bushell *et al.*, 2008). Firstly, recombinant biotinylated RH5 bait was expressed and quantitated by ELISA (Fig. 4.3A). Immunoblot using a streptavidin-HRP probe, detected a protein band at 88 kDa, corresponded to the 63kDa full length RH5 obtained in previous studies, but containing C-terminal tags (Cd4-Biolinker-His) (Rodriguez *et al.*, 2008; Baum *et al.*, 2009) (Fig 4.3B). A smaller product at 70kDa, likely corresponds to the native 45kDa processed fragment of RH5 which was reported previously, was also observed (Baum *et al.*, 2009). A smaller sized fragment, about 28kDa, was also detectable. This band was observed in previous experiments in our laboratory and represents the protein tags (Cd4-Biolinker-His). The latter protein fragment appears to be the result of a cleavage event within a presumed proteolytically prone area, nearby the C-terminus of the RH5 protein ectodomain sequence (section 5.4.1).

Pentameric, soluble, β-lactamase tagged BSG prey was also expressed recombinantly, and the level of expression was estimated by monitoring the turnover of the β-lactamase substrate, nitrocefin, in a time-course assay (Fig 4.3C). The BSG expression level was above the threshold level required for the AVEXIS assay (section 2.5). The RH5 bait was then immobilised on a streptavidin-coated plate and probed against pentameric BSG prey, which was pre-incubated with a dilution series of hybridoma tissue culture supernatant or purified MEM-M6/4 and MEM-M6/8. Purified MEM-M6/4 mAb as well as MEM-M6/4 tissue culture supernatant showed a moderate inhibitory effect at very high concentrations (Fig 4.2D). MEM6-M/8 blocked the interaction at concentrations greater than 100µg/ml, whereas the equivalent tissue culture supernatant had no inhibitory effect (Fig 4.2D).

Considering the published affinity constants of MEM-M6/4 (K_D =6.69x10^{-11} M) and MEM-M6/8 (K_D =5.38x10^{-10} M; Koch *et al.*, 1999) these results were unexpected,

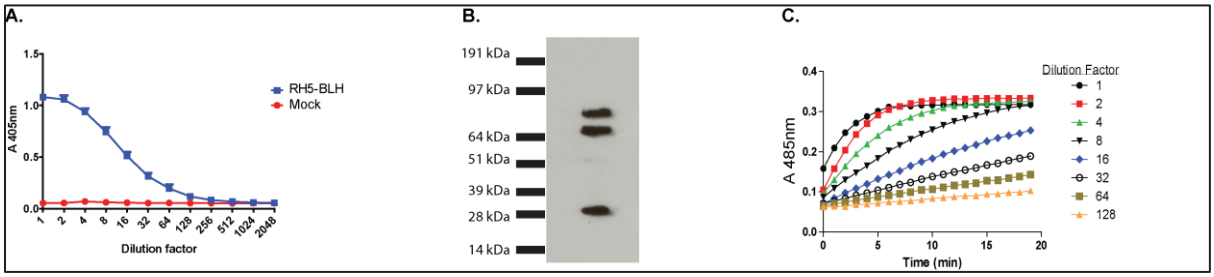

Figure 4.3 Expression of recombinant RH5-BLH and BSG-BLFH.

A. Quantitation of recombinant monomeric RH5-BLH by ELISA (a representative graph is shown). Biotinylated RH5-BLH from tissue culture supernatant was serially diluted and immobilised on a streptavidin-coated plate. The anti-Cd4 mouse monoclonal OX68, was used as the primary antibody and an alkaline phosphatase-conjugated anti-mIgG as the secondary antibody.

B. Immunoblot of recombinant RH5-BLH (a representative blot is shown). Tissue culture supernatant containing RH5-BLH, was resolved under reducing conditions by SDS-PAGE, blotted, and probed using streptavidin-HRP. The two higher molecular weight bands (88kDa and 70kDa) likely correspond to the previously observed 63kDa and 45kDa RH5 products (Baum *et al.*, 2009). The fragment at 28kDa represents the Cd4-BioLinker-His tag which likely derived from proteolytical processing of the RH5-BLH.

C. Quantitation of recombinant pentameric BSG-BLFH (Beta-Lac – Flag – His) by monitoring nitrocefin turnover over time (a representative graph is shown). A dilution series of tissue culture supernatant containing BSG-BLFH was tested in this manner.

raising the possibility that the antibodies had lost a fraction of their activity during the low pH elution stage of protein G purification (section 2.2.9). To exclude such a case, I sought to re-purify the antibodies by a method that avoids the use of low pH, such as precipitation by ammonium sulfate. Therefore, I re-grew the two hybridoma cell lines and collected fresh tissue culture supernatant from where antibodies were salted out of solution using a saturated solution of ammonium sulfate. Ammonium sulfate precipitated antibodies were able to bind BSG *in vitro,* as assessed by ELISA (Fig 4.2C). However, their potency to block the RH5-BSG interaction in AVEXIS did not improve in comparison to protein G purified antibodies (Fig 4.2D). These results suggest that the weak inhibitory effect of protein G purified MEM-M6/4 and MEM-M6/8 on RH5-BSG interaction, was not due to loss of antibody activity, after exposure to low pH.

4.3.3 MEM-M6/4 is able to stain human erythrocytes *in vitro* and to inhibit erythrocyte invasion in parasite culture

To test whether the *in vitro* results could be recapitulated in another system, MEM-M6/4 and MEM-M6/8 were assessed for their ability to block erythrocyte invasion in parasite culture. To this end, a *P. falciparum* culture was sorbitol synchronised and at the late trophozoite to early schizont stage (36-40h post invasion), a dilution series of each antibody was added to the culture and incubated overnight. Consistent with the *in vitro* data (Fig 4.2D), MEM6-M/4 showed a weak blocking effect at high concentrations (Fig 4.2E). MEM6-M/8 did not affect erythrocyte invasion, even when used at high concentrations (Fig 4.2E). It was not, however, clear whether these results were due to the weak or lack of MEM-M6/4 and MEM-M6/8 binding to surface-exposed BSG on human erythrocytes.

To address this question, the binding of MEM-M6/4 and MEM-M6/8 to human erythrocytes was examined. MEM6-M/4 was previously shown to bind to BSG expressed on both resting and activated T-cells whereas MEM-M6/8 was only able to do so, on activated T cells where BSG is up-regulated (Koch *et al.*, 1999). However, none of these antibodies was tested before for their capacity to bind BSG expressed on erythrocytes. Thus, red blood cells were incubated with MEM-M6/4 and MEM-M6/8 followed by incubation with a FITC conjugated anti-mIgG and analysis by flow cytometry. MEM6-M/4 stained human erythrocytes at similar levels

to MEM-M6/6 (positive control) whereas no binding was observed for MEM-M6/8 (Fig 4.2F).

These results suggest that despite the fact that MEM6-M/4 can associate with BSG on human erythrocytes, it is not able to block erythrocyte invasion. It is likely that MEM-M6/4 binds an epitope on BSG which is nearby the RH5 binding site, causing a steric effect to the RH5-BSG interaction which in turn reduces invasion efficiency to a certain level. MEM-M6/8, however, appears unable to bind BSG on the erythrocyte cell surface, most likely due to its low binding affinity (see below) and hence, it has no effect in erythrocyte invasion.

MEM6-M/4 and MEM6-M/8 could not block the RH5-BSG interaction to the level required for the complete abolishment of erythrocyte invasion. Nevertheless, to test whether antibody humanisation by CDR grafting works in my hands, and while the time-consuming work described from section 4.3.7 onwards was ongoing, I decided to humanise and recombinantly express both MEM6-M/4 and MEM6-M/8.

4.3.4 Development of humanised MEM-M6/4 and MEM-M6/8 anti-BSG monoclonal antibodies

An antibody humanisation strategy was designed (shown in Fig 4.4), based on CDR (Complementarity Determining Region) grafting methodology (Jones *et al.*, 1986; Riechmann *et al.*, 1988). Briefly, the protocol is as follows: antibody variable heavy and light chain sequences are amplified and sequenced from the hybridoma line secreting the antibody of interest, followed by CDR sequence identification (Fig. 4.4). The identified CDR sequences are then used to replace the CDRs of the human antibody variable region which is most similar (in the framework region sequences) to the murine CDR donor antibody. The engineered antibody variable region sequences are synthesised by gene synthesis and sub-cloned into the antibody expression plasmid system as described in Chapter 3. Humanised antibodies are then recombinantly expressed in HEK293F cells as described in Chapter 3.

To humanise MEM-M6/4 and MEM-M6/8 it was therefore necessary to sequence and verify the rearranged variable heavy and light chains of each antibody. For this purpose, mRNA was isolated from each hybridoma line, followed by reverse transcription for cDNA synthesis. To amplify antibody variable region

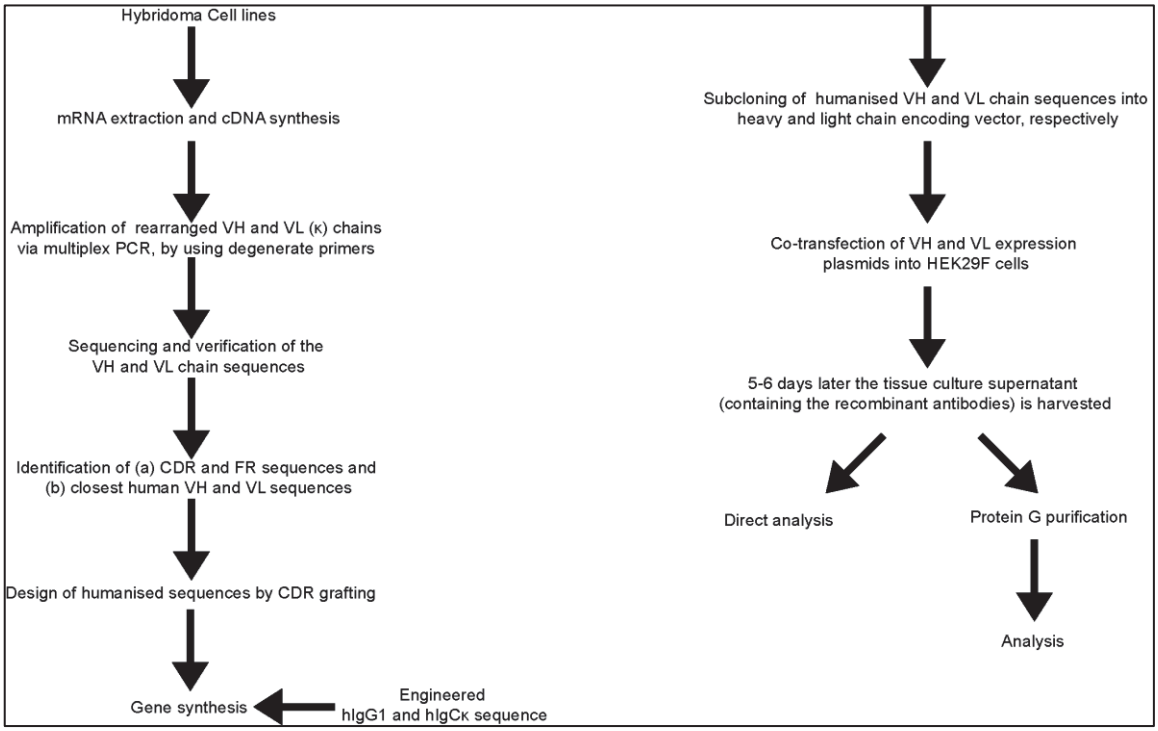

Figure 4.4 A flow chart summarising the strategy that was devised for recombinant humanised antibody development. Abbreviations: VH, Variable Heavy; VL, Variable Light; CDR, Complementarity Determining Region; FR, Framework Region.

sequences, the cDNA was used as substrate in a touchdown multiplex PCR which uses degenerate primers (Crosnier *et al.*, 2010). PCR amplicons were analysed by agarose gel electrophoresis and the DNA contained in the ~400bp bands (Fig 4.5A) was gel extracted, cloned, and sequenced.

The DNA sequencing results were assembled *in silico* and analysed using the IMGT/V-QUEST tool of IMGT database (www.imgt.org). About 80% of the light chain clones sequenced contained the transcribed aberrantly-rearranged light chain of SP2/0 myeloma (Strohal *et al.*, 1987), one of the fusion partners used for the generation of MEM-M6/4 and MEM-M6/8 hybridoma lines (Koch *et al.*, 1999). CDRs and FRs for both MEM-M6/4 and MEM-M6/8 were identified from the other sequences (Fig. 4.5B).

To identify the human variable regions that would serve as acceptors of the mouse CDR sequences, the amino acid sequences of MEM-M6/4 and MEM-M6/8 variable heavy and light chains, were blasted against the human antibody variable region repertoire by using the IMGT/DomainGapAlign tool (www.imgt.org). IGVH3-21*02 and IGHV1-69*04 were identified as the human variable segments having the highest similarity (in the FRs) to MEM-M6/4 and MEM-M6/8 variable heavy chain sequences, respectively. Likewise, IGK1-16*01 and IGK1-39*01 were identified as the closest human variable light chain sequences, for MEM-M6/4 and MEM-M6/8, respectively (Fig. 4.5C). Based on the FR-CDR boundaries set by the IMGT database, murine CDR sequences were engrafted into the chosen human variable region acceptor sequences, replacing the pre-existing CDRs (Fig. 4.5C). The engineered DNA sequences were incorporated downstream of the signal peptide sequence of the respective CDR acceptor chain sequence (Fig. 4.5D), codon optimised for expression in human cells and synthesised by gene synthesis.

4.3.5 Expression and characterisation of humanised MEM-M6/4 and MEM-M6/8 monoclonal antibodies

For recombinant expression of humanised MEM-M6/4 (huMEM-M6/4) and MEM-M6/8 (huMEM-M6/8), synthesised huMEM-M6/4 and huMEM-M6/8 variable heavy and light chain sequences were sub-cloned into the antibody heavy and light chain expression plasmids developed in Chapter 3, followed by transfection in HEK293F cells. Six days post-transfection, tissue culture supernatant was harvested

A.

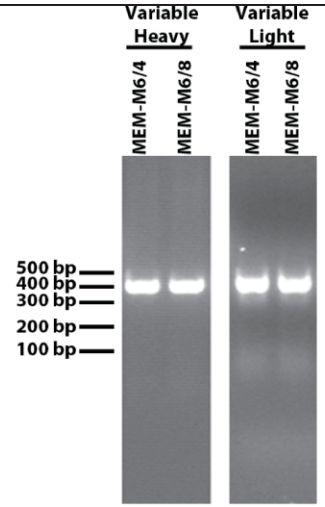

B.

Variable region	FR1	CDR1	FR2	CDR2	FR3	CDR3	FR4
H4	EVQLVESGGGLVKPGGSLKLSCAAS	GFTFSSNA	MSWVRQTPDKRLEWVAT	ISSGSSYN	YYPDNVKGRFTISRDNAKNTLYLQMSSLRSEDTAMYYC	SSRGDNFLFAY	WGQGTLVTVSA
H8	QVQLQQSGAELVRPGASVKLSCKAS	GYTLTDYY	VNWVRQRPGQGLEWIAR	INPGSGNT	YYTENFKGRATLTAEKSSNTAYMQLTSLASEDSAVYFC	ARSELLRYGFDV	WGTGTTVTVSS
L4	DIQMTQSPSSMYASLGERVTITCKAS	QDINSY	LSWFQQKPGKSPKTLIY	RAN	RLVDGVPSRFSGSGSGQDYSLTISSLEFEDLGIYYC	LQFDEFPWT	FGGGTKLEIK
L8	DIQMTQTTSSLSASLGDRVTISCRAS	QDITNY	LNWYQQKPDGTVKLLIY	YTS	RLHSGVPSRFSGSGSGTDFSLTISHLDQEDIATYFC	QQAHTLPPT	FGGGTKLEIK

C.

Variable region	Closest human V region	FR1	CDR1	FR2	CDR2	FR3	CDR3	FR4
H4	IGHV3-21*02	EVQLVESGGGLVKPGGSLRLSCAAS	GFTFSSNA	MNWVRQAPGKGLEWVSS	ISSGSSYN	YYADSVKGRFTISRDNAKNSLYLQMNSLRAEDTAVYYC	SSRGDNFLFAY	WGQGTLVTVSS
H8	IGHV1-69*04	QVQLVQSGAEVKKPGSSVKVSCKAS	GYTLTDYY	ISWVRQAPGQGLEWMGR	INPGSGNT	NYAQKFQGRVTITADKSTSTAYMELSSLRSEDTAVYYC	ARSELLRYGFDV	WGQGTTVTVSS
L4	IGKV1-16*01	DIQMTQSPSSLSASVGDRVTITCRAS	QDINSY	LAWFQQKPGKAPKSLIY	RAN	SLQSGVPSRFSGSGSGTDFTLTISSLQPEDFATYYC	LQFDEFPWT	FGQGTKVEIK
L8	IGKV1-39*01	DIQMTQSPSSLSASVGDRVTITCRAS	QDITNY	LNWYQQKPGKAPKLLIY	YTS	SLQSGVPSRFSGSGSGTDFTLTISSLQPEDFATYYC	QQAHTLPPT	FGGGTKVEIK

D.

Variable region	Closest human V region	Signal peptide sequence
H4	IGHV3-21*02	MELGLRWVFLVAILEGVQC
H8	IGHV1-69*04	MDWTWRFLFVVAAATGVQS
L4	IGKV1-16*01	MDMRVLAQLLGLLLLCFPGARC
L8	IGKV1-39*01	MDMRVPAQLLGLLLLWLRGARC

Figure 4.5 Sequence analysis and humanisation of MEM-M6/4 and MEM-M6/8 variable regions.

A. MEM6-M/4 and MEM6-M/8 variable heavy and light chain sequences were amplified from hybridoma cDNA by multiplex PCR, and analysed by agarose gel electrophoresis. A single band at about 400bp corresponds to the amplified variable heavy or light chain sequences.

B. The amino acid sequences of MEM-M6/4 and MEM-M6/8 mouse rearranged variable regions as derived from sequence analysis of the amplified cDNA sequences.

C. The amino acid sequences of the humanised MEM-M6/4 and MEM-M6/8 variable heavy and light chains after CDR grafting. The amino acid sequences of mouse variable regions were blasted against the human antibody variable region repertoire in IMGT database. Based on the similarity in the framework regions the closest human variable heavy and light regions were identified and served as acceptors of the mouse CDRs.

D. The amino acid sequences of the signal peptides that were incorporated upstream the engineered variable regions.

Abbreviations: CDR, Complementarity Determining Region; FR, Framework Region; H4 and H8, Variable Heavy chains of (hu)MEM-M6/4 and (hu)MEM-M6/8, respectively; L4 and L8, Variable Light chains of (hu)MEM-M6/4 and (hu)MEM-M6/8, respectively.

and analysed for the presence of antibody by western blot (Fig 4.6A). Two bands at 55 and 28kDa, corresponding to antibody heavy and light chain were detected, confirming antibody expression and secretion. Then, the ability of huMEM-M6/4 and huMEM-M6/8 to bind BSG *in vitro* was tested by ELISA. Both unpurified and protein G purified huMEM-M6/4 and huMEM-M6/8 demonstrated binding to BSG in an ELISA assay (Fig. 4.6 B,C).

The capacity of huMEM-M6/4 and huMEM-M6/8 to inhibit the RH5-BSG interaction *in vitro* was also examined in an AVEXIS assay. Pre-incubation of pentameric BSG with a dilution series of either unpurified or protein G purified huMEM-M6/4 and huMEM-M6/8, was insufficient to completely prevent the binding of BSG to RH5 (Fig 4.6D). These data show that MEM-M6/4 and MEM-M6/8 were successfully humanised; recombinantly expressed humanised antibodies retained their capacity to bind BSG *in vitro*. However, similar to the mouse parental antibodies, huMEM-M6/4 and huMEM-M6/8 could not completely inhibit the interaction between RH5 and BSG *in vitro.*

The efficacy of huMEM-M6/4 and huMEM-M6/8 in blocking merozoite invasion was assessed in an erythrocyte invasion assay. HuMEM-M6/4 and huMEM-M6/8 were not able to abolish erythrocyte invasion when included into the culture medium of parasite infected erythrocytes (Fig 4.6E). To further investigate the latter observation, huMEM-M6/4 and huMEM-M6/8 were tested for their binding capacity to human erythrocytes. Both humanised antibodies lacked the ability of staining human erythrocytes *in vitro* as assessed by flow cytometry (Fig 4.6F). These data show that despite retaining their binding specificity, neither huMEM-M6/4 or huMEM-M6/8 could prevent erythrocyte invasion in *P. falciparum* culture, probably due to their inability to bind to erythrocyte exposed BSG.

4.3.6 Biophysical characterisation of mouse and humanised MEM-M6/4 and MEM-M6/8 anti-BSG monoclonal antibodies

As demonstrated earlier in this Chapter, MEM-M6/4 and MEM-M6/8 did not inhibit the RH5-BSG interaction to the level required to prevent erythrocyte invasion. Considering the published affinity constants of both antibodies which are on the same range as the highly efficacious MEM-M6/6 (Koch *et al.*, 1999), these results were surprising. Therefore, I sought to measure the affinities of MEM-M6/4 and

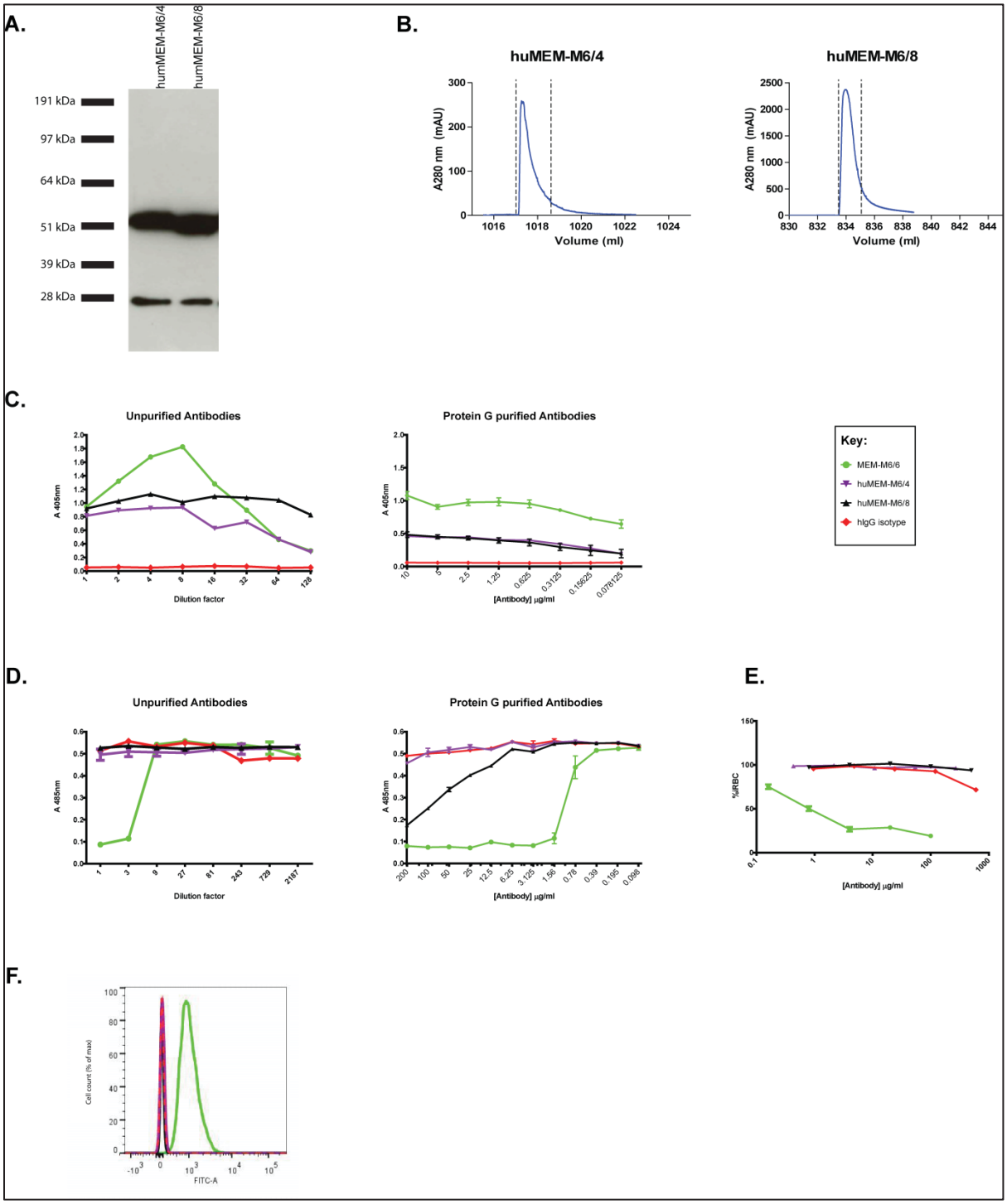
A.
humMEM-M6/4
humMEM-M6/8
191 kDa
97 kDa
64 kDa
51 kDa
39 kDa
28 kDa
B.
huMEM-M6/4
A280 nm (mAU)
Volume (ml)
huMEM-M6/8
A280 nm (mAU)
Volume (ml)
C.
Unpurified Antibodies
A 405nm
Dilution factor
Protein G purified Antibodies
A 405nm
[Antibody] µg/ml
Key:
MEM-M6/6
huMEM-M6/4
huMEM-M6/8
hIgG isotype
D.
Unpurified Antibodies
A 485nm
Dilution factor
Protein G purified Antibodies
A 485nm
[Antibody] µg/ml
E.
%RBC
[Antibody] µg/ml
F.
Cell count (% of max)
FITC-A

Figure 4.6 Characterisation of humanised MEM-M6/4 and MEM-M6/8 antibodies.

A. Humanised heavy and light antibody chains were readily detected in tissue culture supernatant, by western blot. Tissue culture supernatant containing huMEM-M6/4 or huMEM-M6/8 was analysed by denaturing SDS-PAGE, blotted and probed by using a Horseradish Peroxidase conjugated anti-hIgG. Two bands at 55 and 28 kDa were obtained corresponding to antibody heavy and light chain, respectively.

B. HuMEM-M6/4 and huMEM-MEM-6/8 were affinity purified from tissue culture supernatant on protein G column. The eluate in each experiment was monitored at 280 nm in real-time and the peak fractions containing antibodies (between dashed lines) were pooled.

C. BSG was bound by unpurified (left) or protein G purified (right) huMEM-M6/4 and huMEM-M6/8 antibodies, in an ELISA assay. BSG-BLH from tissue culture supernatant was immobilised on a streptavidin-coated plate at concentrations sufficient for complete saturation of the available binding surface, followed by incubated with a 2-fold dilution series of each humanised antibody. An alkaline phosphatase conjugated anti-hIgG was used as secondary.

D. Tissue culture supernatant containing huMEM-M6/4 or huMEM-M6/8 (left) or protein G purified antibodies (right) did not block the interaction between RH5 and BSG, in an AVEXIS assay. RH5-BLH from tissue culture supernatant was immobilised on a streptavidin-coated plate at concentrations sufficient for complete saturation of the available binding surface. Immobilised RH5-BLH was then probed against pentameric β-lactamase tagged BSG-BLFH which was pre-incubated with a dilution series of each antibody.

E. HuMEM-M6/4 and huMEM-M6/8 had no effect in erythrocyte invasion. A synchronised *P.falciparum* culture*,* at the schizont stage, was incubated overnight with a dilution series of each of the humanised antibodies. The infected erythrocytes were then fixed, stained with SYBR Green I and analysed by flow cytometry. The graph shows the percentage of infected red blood cells (iRBC) as a function of antibody concentration.

F. HuMEM-M6/4 and huMEM-M6/8 antibodies did not stain human erythrocytes. Human erythrocytes were incubated with 10µg/ml of each antibody, followed by 1h incubation with a FITC-conjugated anti-hIgG. The binding of huMEM-M6/4 and huMEM-M6/8 to red blood cells was then analysed by flow cytometry. The histogram shows the normalised cell count as a function fluorescence intensity at the FITC emission wavelength.

Data in *C, D* and *E* are shown as mean ± standard error; *n*=3. In all experiments the anti-BSG antibody MEM-M6/6 was used as positive control, and a hIgG isotype as negative.

For clarity reasons *A.* and *C.* (left) are reproduced here from Fig. 3.2.

MEM-M6/8 for BSG by SPR, and compare them with the already published ones as well as with those of the humanised antibody versions.

In the SPR experiments described below, antibodies were immobilised on the sensor chip surface and used as ligands, whereas purified monomeric BSG was used as the analyte. IgG antibodies are dimeric, carrying two antigen binding sites which bind independently to the antigen when the experiment is setup in this orientation (antibody as ligand and BSG as analyte). Using this method, I was able to calculate the kinetic and equilibrium binding parameters based on a simple 1:1 binding model. If the reverse orientation (BSG as ligand and antibody as analyte) was used, the engagement of the two antibody binding sites would not be independent of each other (two state reaction), and this would require the utilization of more complicated mathematical models for the calculation of kinetic and affinity parameters. Therefore, the orientation antibody-ligand and BSG-analyte was preferred.

4.3.6.1 Identifying the appropriate condition for regenerating the sensor chip surface

The interaction between an antibody and its target is normally of high affinity, typically in the nM range, and once the antibody-antigen complex is formed, spontaneous dissociation occurs at slow rates that could take several hours for complete dissociation. In SPR experiments, once the desired measurements are taken, antibody-antigen complexes can be disrupted by using a buffer (regeneration solution) that dissociates the complexes and thereby enabling repeated analyses on the same surface. Such a regeneration solution can vary between different antibody-antigen complexes and the identification of a single condition appropriate for all complexes under investigation is not trivial (Andersson *et al.*, 1999; Hoffman *et al.*, 2000).

By definition, regeneration is the process of removing bound analyte from the surface after an analysis cycle without damaging the ligand, in preparation for a new cycle. Incomplete regeneration or loss of the binding activity from the surface will impair the performance of the assay, and influence the final results (www.gehealthcare.com). Therefore, the ideal regeneration condition would result in consistent analyte responses in repeated cycles (differing less than 5% between

each other), and at the end of each regeneration step, the response should return to the baseline. To identify the ideal regeneration condition capable of dissociating the antibody-antigen complex without affecting the immobilised antibody, a regeneration solution scouting strategy was followed.

First, protein G-purified MEM-M6/4 (Fig. 4.2 A, B) was *in vitro* biotinylated, and immobilised on the surface of a streptavidin-coated (SA) sensor chip. BSG contained in tissue culture supernatant was injected over immobilised MEM-M6/4 and the analyte response was taken. This was followed by the injection of the regeneration solution under investigation, and the recording of the baseline response. To get the overall trend, this cycle was repeated five times for each regeneration condition, and a trend plot was drawn (Fig. 4.7). Two concentrations of NaCl, a single concentration of ethylene glycol, 10mM glycine at pH 2.2 or 2.5 and 100mM H_3PO_4, all proved to be too mild for disrupting the antibody-antigen complex: the baseline never returned to the reference levels and as a consequence the analyte response in the next cycles was reduced. In contrast 10mM glycine at pH 2 and 0.05%SDS were detrimental for the immobilised ligand (Fig. 4.7). Overall, none of the regeneration conditions tested provided acceptable results.

Therefore, I sought to use an alternative sensor chip of which the principle for regenerating the surface would be different from the SA chip. I chose to employ the CAP chip which I felt it would be ideal for the purposes of my experiments. CAP chip uses a ligand-independent regeneration protocol, removing the need of establishing appropriate regeneration conditions (Fig. 4.8A). It is based on a concept that allows for the reversible capture of biotinylated molecules. CAP chip is built on a carboxymethylated dextran matrix to which a single stranded DNA molecule is pre-immobilised. Biotin CAPture Reagent consists of streptavidin conjugated with the complementary single stranded DNA molecule which can hybridize on the sensor chip surface (gehealthcare.com). The biotinylated ligand under investigation can be then immobilised on the CAPture Reagent, followed by the required analysis with the appropriate analyte. Finally, the sensor chip surface is fully regenerated allowing re-immobilisation of fresh ligand for the next experimental cycle (Fig. 4.8A).

To test the reliability of the CAP chip, BSG contained in tissue culture supernatant was injected over biotinylated MEM-M6/4, immobilised on Biotin CAPture reagent. CAP chip demonstrated satisfactory repeatability as three

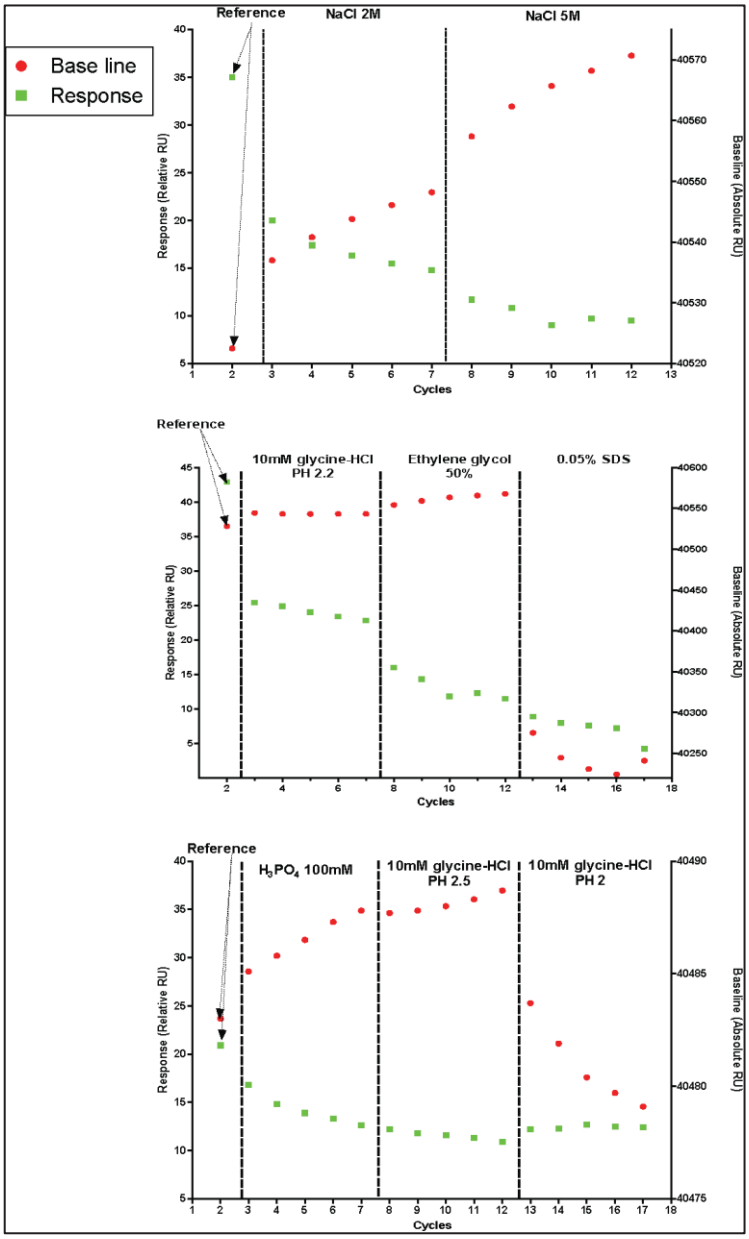

Figure 4.7 Regeneration scouting of SA chip.

Trend plots of regeneration scouting experiment by using an SA chip. MEM-M6/4 was *in vitro* biotinylated and captured on the surface of an SA sensor chip at about 400 response units. Five repeated analyte (BSG) binding and regeneration cycles were tested for each regeneration solution. Report points were set shortly before analyte injection for baseline (red dots) and shortly after sample injection for analyte response (green dots). The points of the second cycle indicate the starting values while each of the subsequent points demonstrates the effects of the previous cycle. Analyte responses were obtained after injecting tissue culture supernatant containing BSG over immobilised antibody, at a flow rate of 20µl/min for 30s. For each injection, the analyte response was plotted relative to the baseline of the previous regeneration cycle. Each graph represents a set of experiments, tested on the same flowcell.

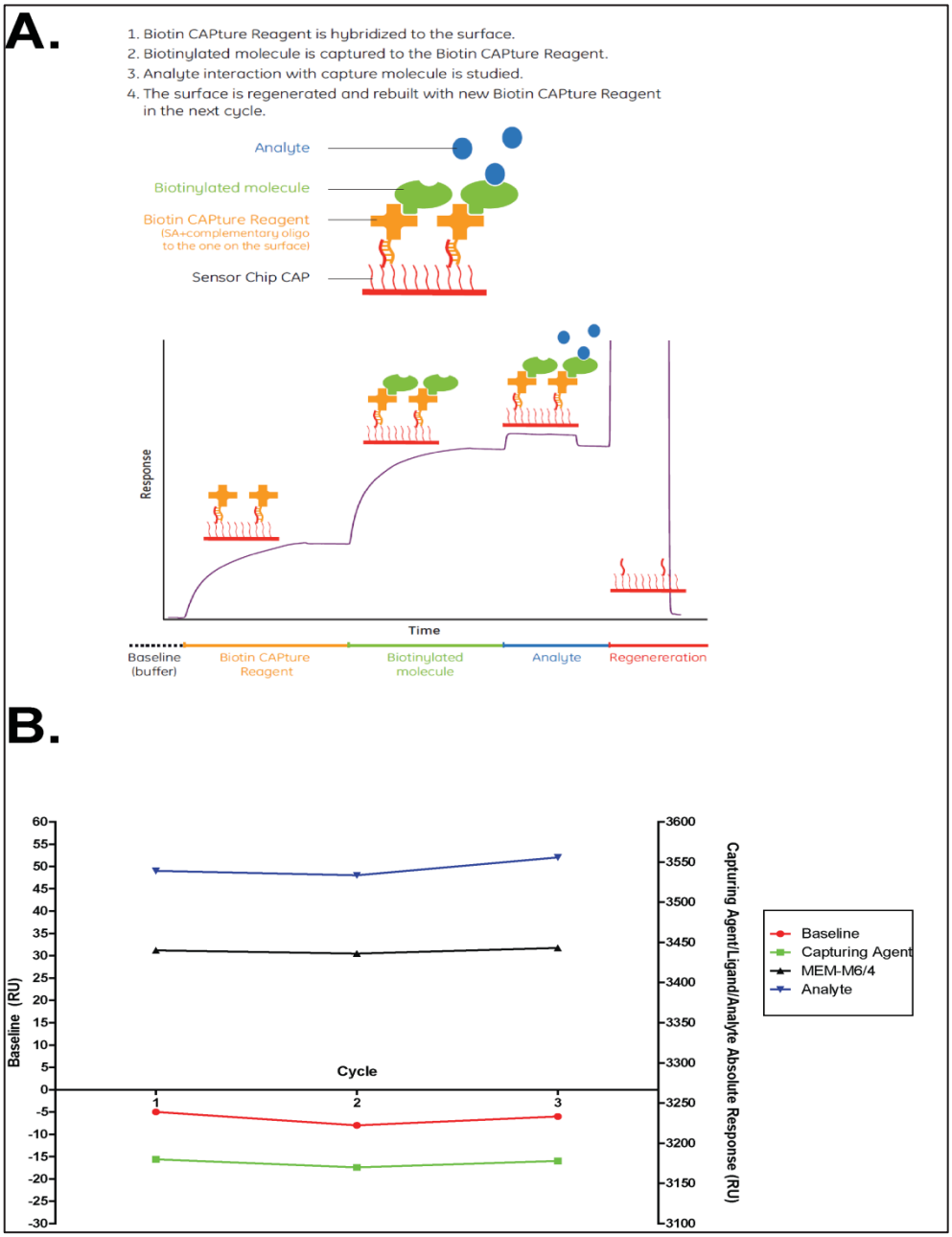

Figure 4.8 CAP chip provides consistent responses after repeated analyte binding and regeneration cycles.

A. A schematic diagram showing the principle on which CAP chip is based (picture adapted from www.gehealthcare.com)

B. Testing the repeatability of CAP chip after three analyte binding and regeneration cycles. The capture reagent was immobilised on the surface of a CAP chip at about 3150 response units followed by capturing of *in vitro* biotinylated MEM-M6/4 at about 300 response units. Analyte responses were obtained after injecting unpurified BSG contained in tissue culture supernatant, over immobilised antibody, at a flow rate of 20µl/min for 30s. The surface was regenerated by using the regeneration solution provided by the manufacturer.

repeated cycles of analyte binding and surface regeneration, gave consistent analyte responses and a steady baseline trend (Fig. 4.8B). Therefore CAP chip was chosen for the subsequent SPR experiments.

4.3.6.2 Measurement of affinity and kinetic parameters of mouse and humanised MEM-M6/4 and MEM-M6/8 antibodies

MEM-M6/4 and MEM-M6/8 as well as their humanised versions, were subjected to biophysical analysis. For this purpose, BSG was recombinantly expressed and purified from tissue culture supernatant by affinity chromatography on a nickel-charged Sepharose column (Fig. 4.9A). The purified protein was then subjected to gel filtration to separate any aggregates that can confound SPR measurements and to exchange the protein into the SPR buffer. The protein eluted from the gel filtration column as a monodisperse peak (Fig. 4.9A). The expected elution volume for BSG monomer was 34.6ml, corresponding to an estimated size of 56.3kDa. The gel filtrated protein was analysed by SDS-PAGE under reducing conditions to confirm its purity and presence at the correct size (Fig. 4.9B).

For the measurement of (hu)MEM-M6/4 and (hu)MEM-M6/8 kinetic parameters, *in vitro* biotinylated antibodies were immobilised on the surface of a CAP chip followed by injection of a dilution series of monomeric BSG across the SPR sensor chip. Each group of sensorgrams was obtained after subtracting the signal of the reference flow cell where the appropriate antibody isotype control was captured (Fig. 4.9C).

A 1:1 Langmuir binding model was separately fitted to the association and dissociation parts of the binding curves, allowing the calculation of association and dissociation rate constants, k_a and k_d respectively (Fig. 4.9C, D). The equilibrium dissociation constant (K_D) *was* calculated after plotting the reference-subtracted maximum responses of each experiment as a function of analyte concentration (Fig. 4.9C, D). The Chi^2 (also known as coefficient of determination or R^2), a measure of the difference between the experimental data and the fitted curve, was taken into account as an indication of the goodness of the fit.

The estimated K_{Ds} for MEM-M6/4 and MEM-M6/8 ($3.93x10^{-8}$M and $1.35x10^{-6}$M respectively) vastly differ to those reported previously ($6.69x10^{-11}$ M and $5.38x10^{-10}$ M respectively; Koch *et al.*, 1999), by 3 to 4 orders of magnitude (Fig. 4.9D).

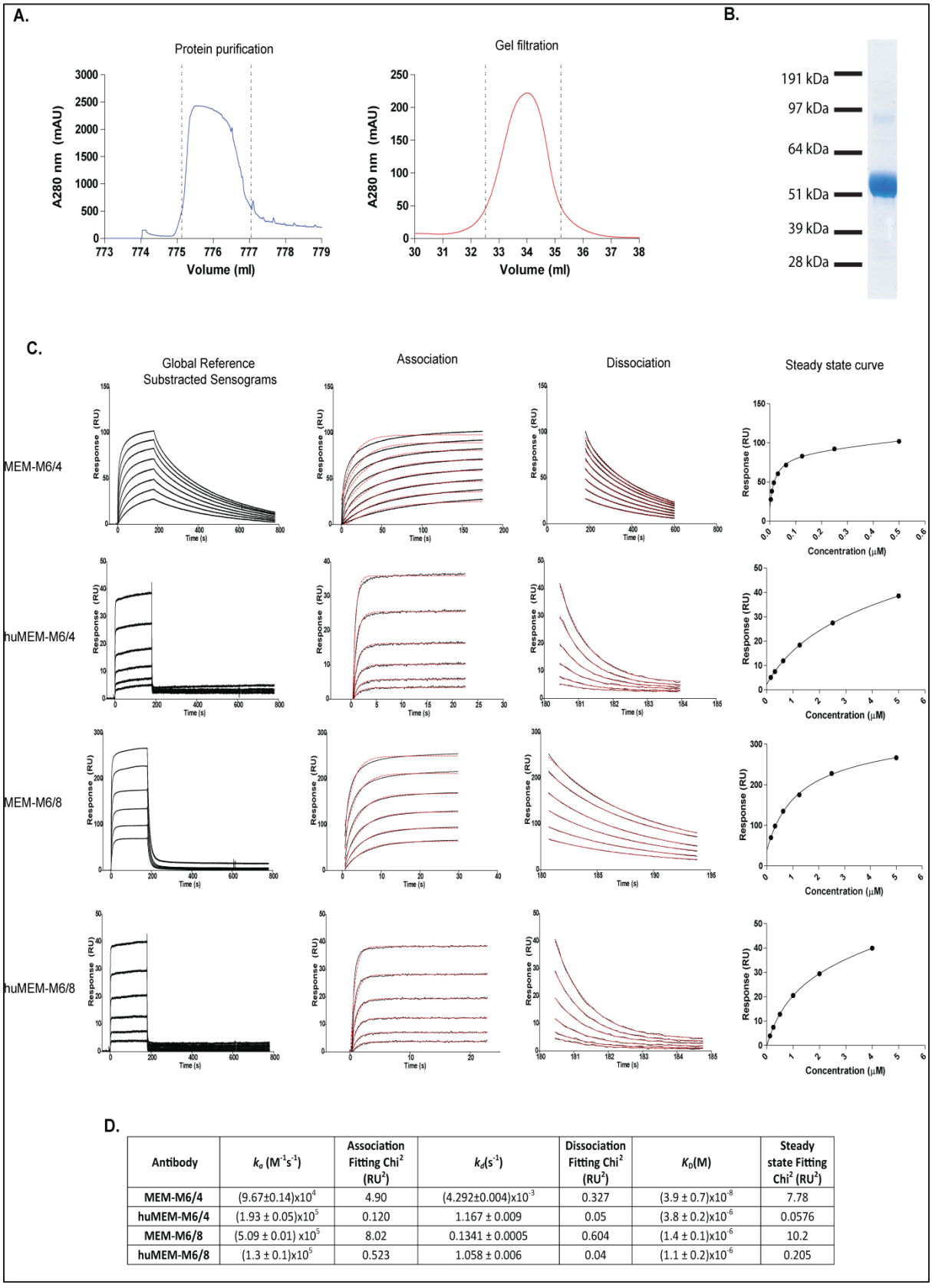

D.

Antibody	k_a ($M^{-1}s^{-1}$)	Association Fitting Chi^2 (RU^2)	k_d(s^{-1})	Dissociation Fitting Chi^2 (RU^2)	K_D(M)	Steady state Fitting Chi^2 (RU^2)
MEM-M6/4	$(9.67\pm0.14)\times10^{4}$	4.90	$(4.292\pm0.004)\times10^{-3}$	0.327	$(3.9\pm0.7)\times10^{-8}$	7.78
huMEM-M6/4	$(1.93\pm0.05)\times10^{5}$	0.120	1.167 ± 0.009	0.05	$(3.8\pm0.2)\times10^{-6}$	0.0576
MEM-M6/8	$(5.09\pm0.01)\times10^{5}$	8.02	0.1341 ± 0.0005	0.604	$(1.4\pm0.1)\times10^{-6}$	10.2
huMEM-M6/8	$(1.3\pm0.1)\times10^{5}$	0.523	1.058 ± 0.006	0.04	$(1.1\pm0.2)\times10^{-6}$	0.205

Figure 4.9 Biophysical analysis of the binding of mouse and humanised MEM-M6/4 and MEM-M6/8 to BSG, by using Surface Plasmon Resonance.

A. BSG-BLH was affinity purified from tissue culture supernatant, on a nickel column (left), followed by gel filtration (right) to separate monomeric BSG from other forms. The eluate in each of the experiments was monitored at 280 nm in real-time and the peak fractions containing protein (between dashed lines) were pooled. The expected gel filtration elution volume was ~34.6ml.

B. Denaturing SDS-PAGE analysis of gel filtrated BSG. The protein was visualised using Coomassie brilliant blue. The expected band size was 56.3 kDa.

C. Reference subtracted sensorgrams (black lines) from the injection of a 2-fold dilution series of BSG (analyte), over the immobilised *in vitro* biotinylated antibodies (ligands). The analyte was injected at a flow rate of 100µl/min, with a contact time of 180s and a dissociation time of 600s. For the calculation of the association (k_a) and dissociation (k_d) rate constants, a simple Langmuir binding model (red dashed lines) was separately fitted to the association and dissociation parts of the reference subtracted sensorgrams. For the calculation of the equilibrium dissociation constants (K_D) reference-subtracted binding data were plotted as a binding curve (steady state curve). The biotinylated antibodies were immobilised on the chip surface at about 600RU. mIgG or hIgG were used as references, accordingly. Concentration range of BSG used in each experiment: MEM-M6/4, 500-3.9nM; MEM-M6/8, 5µM-0.15µM; huMEM-M6/4, 5-0.15µM; huMEM-M6/8, 4-0.125 µM.

D. Tables with the equilibrium and kinetic parameters estimated for the binding of mouse or humanised MEM6-M/4 and MEM6-M/8 to BSG. For each model, the fit to the experimental data is indicated as the Chi^2 value. The calculated values for the K_D, k_a and k_d are indicated with the standard error.

Whereas huMEM-M6/4 lost a fraction of its affinity for BSG in comparison to the mouse original antibody, the affinity of huMEM-M6/8 was fully retained (Fig. 4.9D). Nevertheless, considering that the K_D between an antibody and its target is typically in the nM range, both (hu)MEM-M6/4 and (hu)MEM-M6/8 are low affinity antibodies.

The low affinity of MEM-M6/8 for BSG is likely the reason for the inability of this to antibody stain human erythrocytes and to prevent erythrocyte invasion in parasite culture. Despite the affinity of MEM-M6/4 for BSG being also low, this antibody was able to bind BSG exposed to human erythrocytes. The latter antibody, however, could only moderately inhibit erythrocyte invasion when tested in erythrocyte invasion assays. As mentioned earlier, it is likely that MEM-M6/4 binds an epitope on BSG which is nearby RH5 binding site, causing a steric effect to the RH5-BSG interaction which in turn reduces invasion efficiency to a certain level.

4.3.7 Selection of a mouse anti-BSG monoclonal antibody

As described earlier in this Chapter, two anti-BSG monoclonal antibodies, MEM-M6/4 and MEM-M6/8, were successfully humanised by CDR grafting. Nonetheless, neither parental mouse nor humanised antibodies inhibited the RH5-BSG interaction to the levels required to prevent erythrocyte invasion. Therefore, it was necessary to find an alternative source of anti-BSG antibodies to serve as CDR donors for the development of an anti-BSG humanised antibody, capable of abolishing erythrocyte invasion with high efficacy. In order to maximise the ability to screen for highly efficient antibodies, we decided to create a new panel of anti-BSG monoclonal antibodies, by directly immunising animals and then selecting for high affinity antibodies which are able to potently block erythrocyte invasion.

Following the protocol described in Fig. 4.10A biotinylated BSG-BLH was recombinantly expressed and purified from tissue culture supernatant by affinity chromatography on a nickel loaded Sepharose column (Fig. 4.10B). To confirm that BSG was expressed at the expected size and eluted from the nickel column, the elution peak fraction was analysed by denaturing SDS-PAGE (Fig. 4.10B). A single band at about 56 kDa indicated the presence of BSG in the elution peak fraction. BSG was then used to immunise a five week old BALB/c male mouse, following the prime-boost regime shown in Fig. 4.10A. The immunisation scheme comprised of three injections, of a BSG-TiterMax Gold (adjuvant) emulsion, with a four week

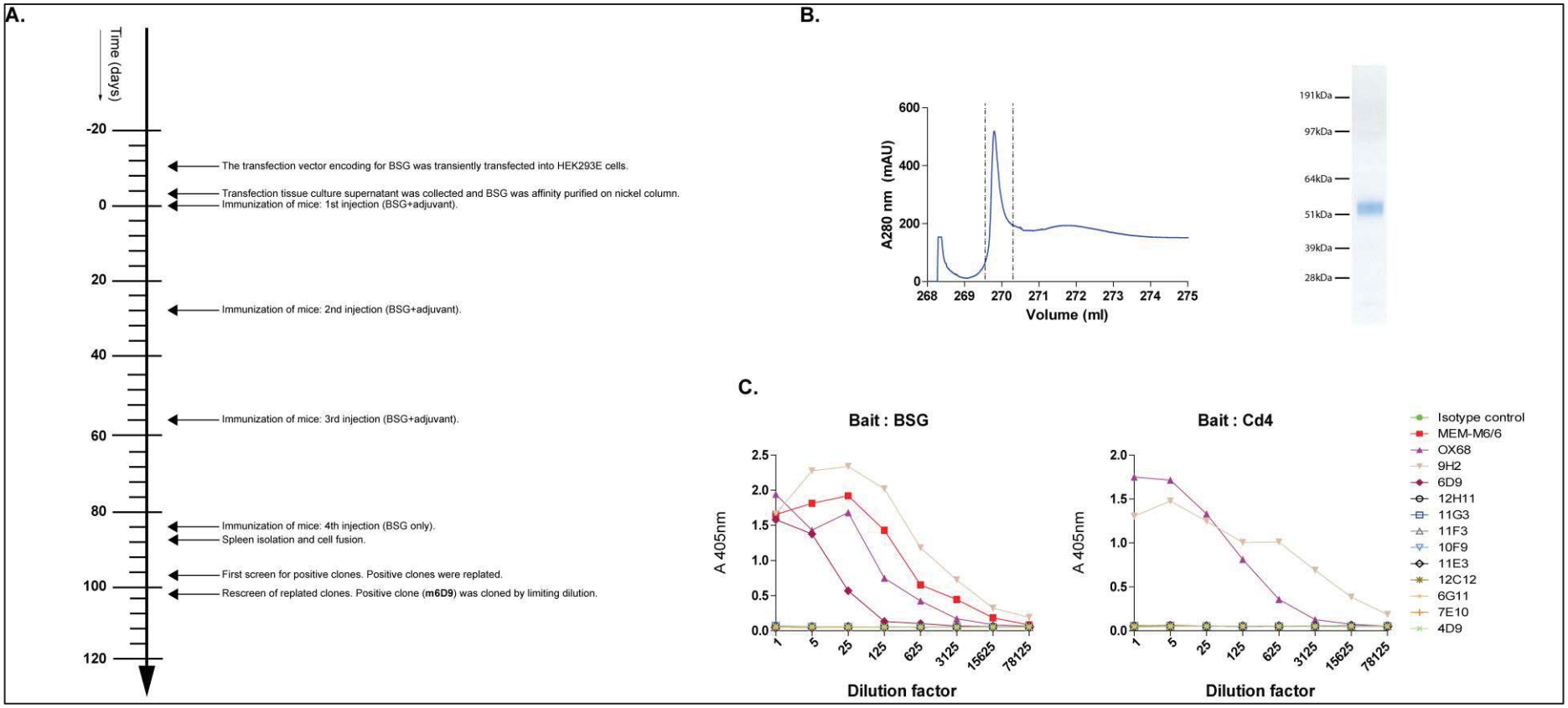
A.
Time (days)
-20
0
20
40
60
80
100
120
The transfection vector encoding for BSG was transiently transfected into HEK293E cells.
Transfection tissue culture supernatant was collected and BSG was affinity purified on nickel column.
Immunization of mice: 1st injection (BSG+adjuvant).
Immunization of mice: 2nd injection (BSG+adjuvant).
Immunization of mice: 3rd injection (BSG+adjuvant).
Immunization of mice: 4th injection (BSG only).
Spleen isolation and cell fusion.
First screen for positive clones. Positive clones were replated.
Rescreen of replated clones. Positive clone (m6D9) was cloned by limiting dilution.
B.
A280 nm (mAU)
600
400
200
0
268
269
270
271
272
273
274
275
Volume (ml)
191kDa
97kDa
64kDa
51kDa
39kDa
28kDa
C.
Bait : BSG
Bait : Cd4
A 405nm
2.5
2.0
1.5
1.0
0.5
0.0
1
5
25
125
625
3125
15625
78125
Dilution factor
Isotype control
MEM-M6/6
OX68
9H2
6D9
12H11
11G3
11F3
10F9
11E3
12C12
6G11
7E10
4D9

Figure 4.10 Overview of the procedure followed for creation and establishment of the hybridoma line m6D9 which secretes an anti-BSG monoclonal antibody.

A. Purified BSG (see *B)*, expressed in HEK293E cells, was used to immunise mice. Hybridomas were generated by cell fusion of splenocytes with SP2/0 myeloma cells, and supernatants were screened for positives by using ELISA (data not shown). Positive clones were re-plated and rescreened. M6D9 was the only positive in the second screen and it was cloned by limiting dilution.

B. The purification traces of BSG (left) as monitored by obtaining the absorbance at 280nm. Peak fractions containing the protein (between the dashed lines) were pooled, analysed by denaturing SDS-PAGE and visualised using Coomassie brilliant blue (right). The expected band size was 56.3 kDa.

C. Hybridoma tissue culture supernatants were tested for the presence of anti-BSG antibodies by ELISA. Biotinylated BSG or Cd4 from tissue culture supernatant were immobilised on a streptavidin-coated plate at concentrations sufficient for complete saturation of the available binding surface, followed by incubation with a five-fold dilution series of each hybridoma supernatant. An alkaline phosphatase-conjugated anti-mIgG antibody was used as secondary antibody. 6D9 hybridoma supernatant was immunoreactive against BSG, whereas 9H2 hybridoma supernatant contained a mAb which bound Cd4 tag.
The anti-BSG MEM-M6/6 or the anti-Cd4 OX68 monoclonal antibodies and a mIgG isotype were used as positive and negative controls, respectively (all at starting concentration 1µg/ml).

interval between injections. Four weeks after the last injection, the mouse was boosted with an additional injection of BSG without adjuvant and left for another three days before the spleen was isolated and dissociated to single cells, which were then fused to SP2/0 myeloma cells.

Ten days after fusion, hybridoma tissue culture supernatants were screened for the presence of anti-BSG antibodies by ELISA. The cell culture supernatant of 11 hybridoma clones (9H2, 6D9, 12H11, 11G3, 11F3, 10F9, 11E3, 12C12, 6G11, 7E10, 4D9) was reactive against BSG and negative against Cd4 tag (data not shown; the ELISA screen experiment was entirely done by Dr Nicole Muller-Sienerth and Dr Nicole Staudt). All eleven clones were re-plated in a 48 well plate and rescreened five days later. Out of eleven initially positive clones, nine clones were negative (12H11, 11G3, 11F3, 10F9, 11E3, 12C12, 6G11, 7E10, 4D9) in the rescreen, one secreted antibodies against the Cd4 tag (9H2), and one (6D9) remained positive (Fig. 4.10 C; Dr Nicole Muller-Sienerth and Dr Nicole Staudt are credited for contributing in animal immunisation, cell fusion and first ELISA screen for positive clones). These results show that a hybridoma line secreting an anti-BSG monoclonal antibody was successfully established.

4.3.8 Characterisation of m6D9 anti-BSG monoclonal antibody

Mouse 6D9 (m6D9) hybridoma was cloned by limiting dilution and after further expansion, m6D9 mAb was purified from cell culture supernatant by affinity chromatography on a protein G column (Fig. 4.11A). Purified m6D9 retained its ability to bind to BSG by ELISA (Fig. 4.11B). The isotype of m6D9 was determined by using an IsoQuiCκ strip (as described in materials and methods) and was found to be an IgG2A (Fig. 4.11C). To test whether m6D9 was able to block the RH5-BSG interaction *in vitro* in AVEXIS, biotinylated RH5 bait was immobilised on a streptavidin-coated plate and probed with β-lactamase tagged BSG pentamer prey, which was pre-incubated with a dilution series of purified m6D9. M6D9 was able to block the interaction between RH5 and BSG with efficacy levels similar to MEM-M6/6 which was used as positive control (Fig. 4.11D).

The ability of m6D9 to inhibit erythrocyte invasion was tested by *P. falciparum* growth inhibition assay. A parasite culture was synchronised by sorbitol treatment and 36-40 hours post invasion a dilution series of m6D9 was added into the culture

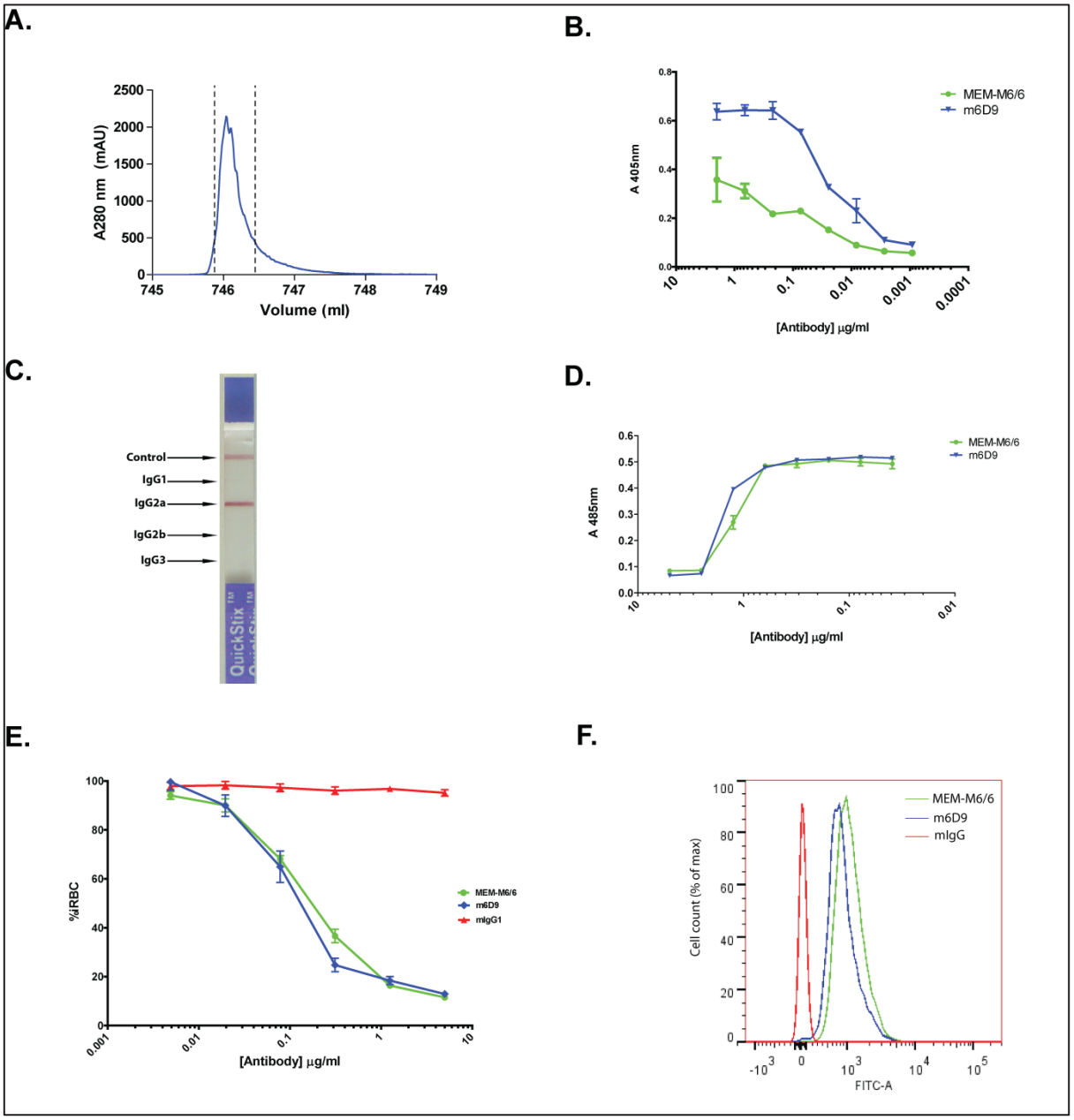
A.
A280 nm (mAU)
2500
2000
1500
1000
500
0
745
746
747
748
749
Volume (ml)
B.
A 405nm
0.8
0.6
0.4
0.2
0.0
10
1
0.1
0.01
0.001
0.0001
[Antibody] µg/ml
MEM-M6/6
m6D9
C.
Control
IgG1
IgG2a
IgG2b
IgG3
QuickStix
D.
A 485nm
0.6
0.5
0.4
0.3
0.2
0.1
0.0
10
1
0.1
0.01
[Antibody] µg/ml
MEM-M6/6
m6D9
E.
%iRBC
100
80
60
40
20
0
0.001
0.01
0.1
1
10
[Antibody] µg/ml
MEM-M6/6
m6D9
mIgG1
F.
Cell count (% of max)
100
80
60
40
20
0
-10^3
0
10^3
10^4
10^5
FITC-A
MEM-M6/6
m6D9
mIgG

Figure 4.11 Characterisation of m6D9 monoclonal antibody.

A. M6D9 was affinity purified from hybridoma tissue culture supernatant, on protein G column. The eluate was monitored at 280 nm in real-time and the peak fractions containing antibody (between dashed lines) were pooled.

***B*.** Protein G purified m6D9 bound to BSG, in an ELISA assay. BSG-BLH from tissue culture supernatant was immobilised on a streptavidin-coated plate at concentrations sufficient for complete saturation of the available binding surface. A dilution series of purified m6D9 was used as primary antibody and an anti-mouse IgG conjugated with alkaline phosphatase as secondary.

C. M6D9 is IgG2A isotype as determined by using an IsoQuiCκ strip.

D. M6D9 blocked the interaction between RH5 and BSG interaction in an AVEXIS assay**.** RH5-BLH from tissue culture supernatant was immobilised on a streptavidin-coated plate and probed against pentameric β-lactamase tagged BSG which was pre-incubated with a dilution series m6D9.

E. Purified m6D9 and was very potent in interfering with erythrocyte invasion when included into the medium of *P.falciparum* infected erythrocytes. A synchnonised parasite culture (schizonts) was incubated overnight with a dilution series of m6D9 followed by fixing, staining and analysis by flow cytometry. The graph shows the percentage of infected red blood cells (iRBC) as a function of antibody concentration.

F. Purified m6D9 stained human erythrocytes. Red blood cells were incubated with m6D9, followed by incubation with a FITC-conjugated anti mouse-IgG secondary and analysis by flow cytometry. The histogram shows the normalised cell count as a function fluorescence intensity at the FITC emission wavelength.

Data in *B, D* and *E* are shown as mean ± standard error; *n*=3. Where applicable the anti-BSG antibody MEM-M6/6 was used as positive control, and a mIgG isotype as negative.

medium and incubated overnight. Cultured erythrocytes were then fixed, stained and analysed by flow cytometry. M6D9 prevented erythrocyte invasion at the levels similar to the positive control antibody MEM-M6/6 (Fig. 4.11 E). To ensure that the blocking mechanism involved the masking of BSG exposed on the surface of red blood cells by m6D9, the binding of m6D9 to erythrocytes was tested by flow cytometry. M6D9 was capable of binding to erythrocytes at levels comparable to MEM-M6/6 positive control (Fig. 4.11F).

These data demonstrate that m6D9 is a high efficacy antibody which blocks the interaction between RH5 and BSG *in vitro,* and prevents erythrocyte invasion in parasite culture. Therefore, it was considered a suitable antibody to serve as CDR donor for the development of an anti-BSG humanised antibody

4.3.9 Development of hu6D9, a humanised anti-BSG monoclonal antibody

The procedure followed for the development of a humanised version of m6D9 (hu6D9), was the same as the one described in section 4.3.4. Sequence analysis of the m6D9 V region sequences (Fig. 4.12A) identified IGHV1-3*01 and IGKV3-15*01 as the human variable segments displaying the highest sequence similarity in FRs to m6D9 variable heavy and light chains sequences, respectively (Fig. 4.12B).

Interestingly, m6D9 variable heavy chain had a cysteine residue within CDR2 (position 58, IMGT numbering) (Fig 4.12A), which was in addition to the two canonical cysteine residues already in place in FR1 and FR3 (positions 23 and 104, IMGT numbering), found in the vast majority of immunoglobulin superfamily domain sequences. While the additional cysteine appears to be a result of affinity maturation of m6D9, it may cause problems in the formation of the correct disulfide bonds in the humanised antibody. Nevertheless, the additional cysteine was retained in the humanised sequence, hoping that it will not cause any conformational issues. Thus, for the development of a humanised 6D9 variable heavy chain (huVH), the CDRs from m6D9 variable heavy chain were engrafted into human IGHV1-3*01 FRs (Fig. 4.12B).

A predicted N-linked glycosylation site within the FR2 of m6D9 variable light chain further complicated the analysis (Fig. 4.12A). This site was to be removed during humanisation by CDR grafting, since all the original FR sequences are replaced by those of the closest human V allele. The size of the putatively attached

A.

Variable region	FR1	CDR1	FR2	CDR2	FR3	CDR3	FR4
VH	EVQLQQSGPELVKTGASVKISCKA	GYSFSDDY	MHWVKQSHGKSLEWIGY	ISCYNGVP	SYNQKFKGKATFTVDTSSSTAYMQFSSLTSEDSAVYYC	ARGGNHGFYYHAMDY	WGQGTSVTVSS
VL	DIVLTQSPAILSVSPGERVSFSCRAS	QSIGTG	IHWYQQRTNGSPRLLIK	FAS	ESISGIPSRFSGSGSGTDFTLSINSVESEDIADYFC	QQSTSWPYT	FGGGTKLEIK

B.

Variable region	Closest human V region	FR1	CDR1	FR2	CDR2	FR3	CDR3	FR4
huVH	IGHV1-3*01	QVQLVQSGAEVKKPGASVKVSCKAS	GYSFSDDY	MHWVRQAPGQRLEWMGW	ISCYNGVP	KYSQKFQGRVTITRDTSASTAYMELSSLRSEDTAVYYC	ARGGNHGFYYHAMDY	WGQGTTVTVSS
huVL	IGKV3-15*01	EIVMTQSPATLSVSPGERATLSCRAS	QSIGTG	LAWYQQKPGQAPRLLIY	FAS	TRATGIPARFSGSGSGTEFTLTISSLQSEDFAVYYC	QQSTSWPYT	FGQGTKLEIK
huVLNTCHFR2		EIVMTQSPATLSVSPGERATLSCRAS	QSIGTG	IHWYQQRTNGSPRLLIK	FAS	TRATGIPARFSGSGSGTEFTLTISSLQSEDFAVYYC	QQSTSWPYT	FGQGTKLEIK

C.

Variable region	Closest human V region	Signal peptide sequence
huVH	IGHV3-1*01	MDWTWRILFLVAAATGAHS
huVL or huVLNTCHFR2	IGHV3-15*01	MEAPAQLLFLLLLWLPDTTG

D.

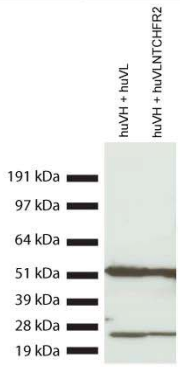

E.

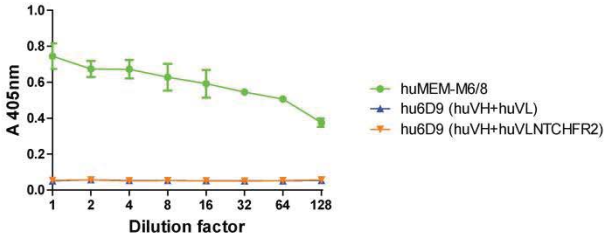

F.

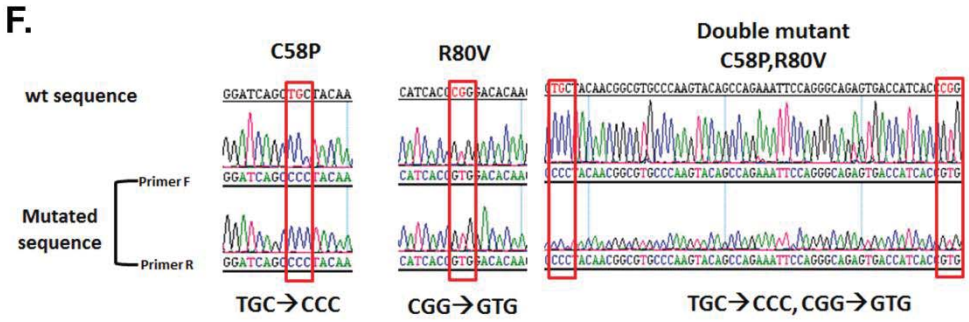

G.

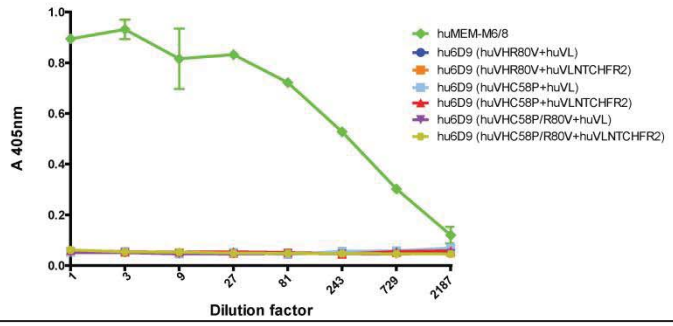

Figure 4.12 Sequence analysis and humanisation of m6D9 by CDR grafting.

A. Sequence analysis and verification of m6D9 variable regions. The table shows the amino acid sequence of m6D9 rearranged variable heavy (VH) and light (VL) chains as derived from sequence analysis of the amplified variable regions. Of note is the N-linked glycosylation site (green) in FR2 of light chain, and the additional cysteine (red) in heavy chain CDR2. The valine at position 80 (IMGT numbering) of the variable heavy chain is shown in blue.

B. The table shows the amino acid sequences of hu6D9 variable heavy (huVH) and light chain, after CDR grafting. Because an N-linked glycosylation site exists within the second FR of m6D9 (see *A.*), two different humanised variable light chains were synthesised: one retaining m6D9 FR2 intact (huVLNTCHFR2), and one exchanging it with the equivalent region of the closest human allele (huVL). The arginine at position 80 (IMGT numbering) of the variable heavy chain is shown in blue.

C. The amino acid sequences of the signal peptides that were incorporated upstream the engineered variable regions.

D. Western blot showing recombinant expression of hu6D9. Supernatants containing antibodies were harvested, resolved under reducing conditions by SDS-PAGE, blotted, and probed using an HRP conjugated anti-hIgG. Two bands at 55 and 28 kDa were obtained corresponding to the antibody heavy and light chain, respectively.

E. Hu6D9 lost an important fraction of its affinity for BSG, as assessed by ELISA.

F. Sequencing chromatographs which confirm the mutations introduced in hu6D9 variable heavy chain.

G. None of the hu6D9 mutants restored affinity for BSG as demonstrated by ELISA.

Data in *E* and *G* are shown as mean ± standard error; n=3.

carbohydrate and how this interplays with the protein moiety is unpredictable, and random removal of the N-linked glycosylation site may affect V region tertiary structure and consequently antibody affinity. Hence, two different humanised variable chains were designed. In the first, m6D9 variable light chain was fully humanised (huVL) by engrafting the mouse CDRs into human IGKV3-15*01 FRs (Fig. 412B). In the second humanised sequence (huNTCHFR2), only FR1, FR3 and FR4 were exchanged, keeping the original mouse FR2 sequence intact. As a result, the N-linked glycosylation site was retained.

Hu6D9 engineered DNA sequences were incorporated downstream of the signal peptide sequence of the respective CDR acceptor chain sequence (Fig. 4.12C), codon optimised for expression in human cells and synthesised by gene synthesis.

4.3.10 Characterisation of hu6D9 humanised anti-BSG antibody

For recombinant expression of hu6D9, synthesised variable heavy and light chain sequences were sub-cloned into the antibody heavy and light chain expression plasmids developed in Chapter 3, followed by transfection in HEK293F cells. Six days later, tissue culture supernatant was analysed by Western blot for the presence of antibody. Two bands at 55 and 28 kDa corresponding to antibody heavy and light chain respectively, confirmed recombinant antibody expression of both hu6D9 versions (huVH+huVL and huVH+huVLNTCHFR2) (Fig. 4.12D). The ability of hu6D9 to bind BSG was tested by ELISA. Neither of the two hu6D9 variants was reactive against BSG (Fig. 4.12E), suggesting that hu6D9 has lost a significant fraction of its affinity for BSG during humanisation.

CDR grafted antibodies often exhibit greatly reduced or completely abolished binding affinity as a consequence of incompatibility of non-human CDRs with human FRs (Lo, 2004; Almagro and Fransson, 2008). The affinity can be partially or fully restored, only after re-introducing some of the parental murine FR residues. Nevertheless, the identification of such residues is not straight forward and requires skills in structural biology and *in silico* three dimensional modelling which is beyond the expertise of my laboratory. Hence, as an alternative I sought to mutate the apparent amino acid residue which may have caused incompatibilities between non-human CDRs and human FRs, the cysteine at position 58 (C58; IMGT numbering).

Sequence analysis of m6D9 VH, revealed that it belongs to the mouse IGHV1 subgroup of V regions and it is most similar to IGHV1-31*01. Closer examination of mouse IGHV1 subgroup, demonstrated that 148 out of 155 (95.48%) mouse V alleles classified as IGHV1 (including IGHV1-31*01) in IMGT database, had proline at position 58 (IMGT numbering) of the CDR2, instead of the cysteine in m6D9 VH. Therefore, it was reasonable to assume that mutating cysteine at position 58 (IMGT numbering) to proline might be beneficial for the antibody affinity.

Another amino acid which was potentially involved in the loss of hu6D9 affinity for BSG, was a valine residue in FR3 (position 80 by IMGT numbering, position 71 by Kabat numbering) of m6D9 VH (Fig 4.12A). The positioning and conformation of heavy chain CDR2, has been proposed to be largely dependent on the nature of the amino acid residue that occupies the position 80 of heavy chain FR3, and changes in this amino acid during humanisation may result in displacement of CDR2 (Tramontano *et al.*, 1990). In huVH, the valine at position 80 had been replaced by an arginine (R80). Considering that CDR2 also contains an unusual cysteine, the V80R substitution may have altered CDR2 conformation in a way that disrupts disulfide bond formation, and therefore affecting the correct folding of the variable heavy chain.

To test whether C58 and/or R80 affected antibody binding, I mutated these amino acids to proline and valine respectively. By using site directed mutagenesis, single (C58P or R80V) and double mutants (C58P/R80V) of huVH were generated (Fig. 4.12F). A number of hu6D9 variants were expressed by co-transfecting different combinations of heavy and light chain encoding vectors into HEK293F cells. Hu6D9 variants, contained in tissue culture supernatant, were then tested for binding to BSG by ELISA. None of the hu6D9 mutants bound to BSG (Fig. 4.12G), suggesting that either more radical changes are likely required to restore hu6D9 affinity for BSG, or the loss of affinity is not reversible.

4.3.11 Development and characterisation of ch6D9, a chimeric anti-BSG monoclonal antibody

Humanisation of m6D9 resulted in a problematic hu6D9, which had lost a significant fraction of its affinity for BSG. Attempts to restore affinity by mutating certain amino acid residues in hu6D9 variable heavy chain were unsuccessful. Thus,

the antibody chimerisation approach was adopted, as an alternative to humanisation. To this end, m6D9 variable heavy and light chain sequences (Fig. 4.12A) were codon optimised, incorporated downstream of the respective heavy and light chain signal peptide sequences shown in Fig 4.12C, and synthesised by gene synthesis. For recombinant expression of chimeric 6D9 (ch6D9), synthesised DNA sequences were sub-cloned into the antibody heavy and light chain expression plasmids developed in Chapter 3, followed by transfection in HEK293F cells. Six days post transfection, tissue culture supernatant was collected and ch6D9 was purified by affinity chromatography on protein G loaded Sepharose column (Fig 4.13A). Protein G purified ch6D9 was able to bind BSG *in vitro,* as shown by ELISA (Fig 4.13B).

The ability of ch6D9 to block the interaction between RH5 and BSG *in vitro*, was assayed by AVEXIS. Ch6D9 exhibited potent blocking capacity, at levels similar to the MEM-M6/6 positive control (Fig. 4.13C). To validate this result, the efficacy of ch6D9 to inhibit *P. falciparum* erythrocyte invasion was assessed in a parasite growth inhibition assay. Ch6D9, neutralized erythrocyte invasion in a dose dependent manner, in all *P. falciparum* strains tested (3D7, Gb4, HB3 Dd2). The efficacy of ch6D9 to inhibit erythrocyte invasion was analogous to MEM-M6/6 positive control (Fig. 4.13D). These results suggest that ch6D9 is a high efficacy antibody and can be considered for therapeutic purposes.

4.3.11.1 Ch6D9 demonstrates reduced binding to FcγRIIA and C1q

The plasmid system for recombinant expression of antibodies described in Chapter 3, was primarily designed for the development and expression of engineered anti-BSG antibodies with therapeutic potential. Such antibodies aim to prevent erythrocyte invasion by inhibiting the interaction between RH5 and BSG. However, the trigger of ADCC and CDC antibody effector functions (section 1.4.2) would be undesirable and detrimental, since the human host would recognise itself as foreign. To eliminate the side effects arising from the stimulation of antibody effector functions, several previously characterised mutations (E233P / L234V / L235A / G236Δ / A327G / A330S/P331S) were introduced to the Fc region of hIgG1 which was incorporated into the heavy chain expression vector (Armour *et al.*, 1999, 2003, 2006). Moreover, to avoid allotype rejection phenomena, the mutations K214T/D356E/L358M (Greenwood and Clark, 1993; Armour *et al.*, 2006) were also introduced to the the Fc region of hIgG1 during gene synthesis (Chapter 3).

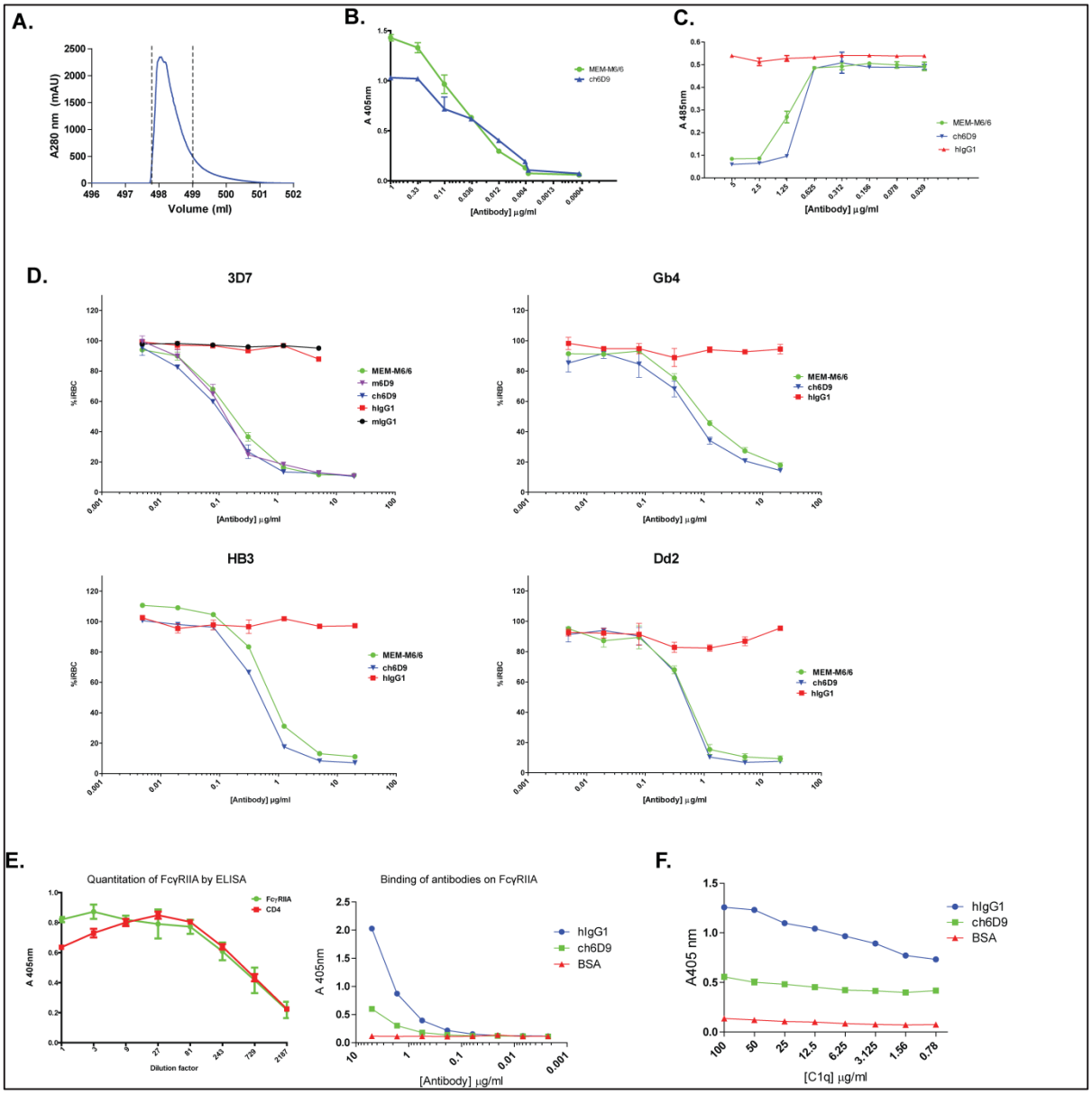
A.
A280 nm (mAU)
Volume (ml)
B.
A 405nm
MEM-M6/6
ch6D9
[Antibody] µg/ml
C.
A 495nm
MEM-M6/6
ch6D9
hIgG1
[Antibody] µg/ml
D.
3D7
%iRBC
MEM-M6/6
m6D9
ch6D9
hIgG1
mIgG1
[Antibody] µg/ml
Gb4
MEM-M6/6
ch6D9
hIgG1
HB3
MEM-M6/6
ch6D9
hIgG1
Dd2
MEM-M6/6
ch6D9
hIgG1
E.
Quantitation of FcγRIIA by ELISA
FcγRIIA
CD4
A 405nm
Dilution factor
Binding of antibodies on FcγRIIA
hIgG1
ch6D9
BSA
A 405nm
[Antibody] µg/ml
F.
hIgG1
ch6D9
BSA
A405 nm
[C1q] µg/ml

Figure 4.13 Development and characterisation of ch6D9 chimeric anti-BSG monoclonal antibody.

A. Ch6D9 was expressed recombinantly and affinity purified from tissue culture supernatant on a protein G column. The eluate was monitored at 280 nm in real-time and the peak fractions containing antibody (between dashed lines) were pooled.

***B*.** Protein-G purified ch6D9 bound to BSG, in an ELISA assay. BSG-BLH from tissue culture supernatant was immobilised on a streptavidin-coated plate at concentrations sufficient for complete saturation of the available binding surface. A dilution series of purified ch6D9 was used as primary antibody and an anti-human IgG conjugated with alkaline phosphatase as secondary.

C. Ch6D9 blocked the interaction between RH5 and BSG interaction, in AVEXIS**.** RH5-BLH from tissue culture supernatant was immobilised on a streptavidin-coated plate and probed against pentameric β-lactamase tagged BSG which was pre-incubated with a dilution series of protein G purified ch6D9.

D. Purified ch6D9 blocked erythrocyte invasion in all *P. falciparum* strains tested**.** A synchronised parasite culture (schizonts) for each of the 3D7, Gb4, HB3 and Dd2 strains, was incubated overnight with a dilution series of ch6D9 followed by fixing, staining and analysis by flow cytometry. In 3D7 culture, m6D9 was also tested for comparison. The graph shows the percentage of infected red blood cells (iRBC) as a function of antibody concentration.

E. Ch6D9 demonstrated reduced binding to FcγRIIA$_{131HIS}$ (right). FcγRIIA α-chain was expressed recombinantly as monomeric biotinylated form and quantitated by ELISA (left). The anti-Cd4 monoclonal antibody OX68 was used as primary antibody and biotinylated Cd4 was used as reference. To test FcγRIIA binding to ch6D9 (right), a dilution 1:9 of tissue culture supernatant containing FcγRIIA was used to immobilise FcγRIIA on a 96 well streptavidin-coated plate. Immobilised FcγRIIA was incubated with a dilution series of ch6D9 or hIgG1 or BSA (negative control). For probing a donkey anti-hIgG F(ab)$_2$ fragment conjugated with alkaline phosphatase was used.

F. Ch6D9 demonstrated reduced binding to C1q, in an ELISA-based assay. Equal amounts of ch6D9 or hIgG1 or BSA (negative control) were adsorbed on a 96 well plate, and incubated with a dilution series of human C1q. Then, the plates were incubated with a goat anti-hC1q followed by a rabbit anti-goat conjugated with alkaline phosphatase. Where applicable, the anti-BSG monoclonal antibody MEM-M6/6 was used as positive control. Data in *B, C, D, E* and *F* are shown as mean ± standard error; *n*=3.

To test whether the mutations carried by hIgG1 Fc region were functional, the binding of ch6D9 to $FcγRIIA_{131His}$ was examined. A vector encoding for a biotinylatable form of human FcγRIIA α-chain (P12318) (provided by Dr Yi Sun), was transfected into HEK293E cells. Five days later, the amount of recombinant biotinylated FcγRIIA present in tissue culture supernatant was evaluated by ELISA (Fig. 4.13E). To test whether the binding of ch6D9 to FcγRIIA was diminished, a saturating amount of FcγRIIA was immobilised on a streptavidin coated plate and incubated with a dilution series of ch6D9 or wild type (non-mutated) hIgG1 isotype, followed by probing with an alkaline phosphatase conjugated anti-hIgG $F(ab)_2$ secondary. Ch6D9 demonstrated reduced binding to FcγRIIA in comparison to hIgG1 reference (Fig. 4.13E), providing evidence that the mutations in ch6D9 Fc region are functional in terms of eliminating Fcγ receptor binding. Ideally, the interaction between ch6D9 and other Fcγ receptors would have also been assayed, but attempts to get access to a panel of Fcγ expression constructs optimized for recombinant expression in HEK293 cells (Shields *et al.*, 2001), were unsuccessful.

The activation of the classical complement pathway by ch6D9 was also examined by assaying for its ability to recruit human C1q, in an ELISA based assay. A fixed amount of ch6D9 or unmodified hIgG1 isotype was adsorbed on the plastic bottom of a 96-well plate and incubated with a dilution series of human C1q. The plate was then washed to remove unbound C1q, followed by serial incubation with goat anti-human C1q and rabbit anti-goat IgG conjugated with alkaline phosphatase. The amount of C1q bound to ch6D9 was reduced in comparison to hIgG1 (Fig. 4.13F), suggesting an impaired capability of ch6D9 to activate the classical pathway of complement cascade.

These results demonstrate that the mutations introduced in ch6D9 Fc region are functional, and thus, suggest that ch6D9 is likely to have impaired ability to trigger ADCC and CDC antibody effector functions.

4.3.11.2 Epitope mapping of ch6D9 on BSG

To further characterise ch6D9, I attempted to map ch6D9 epitope on BSG by using an array of BSG constructs previously generated in the lab (by Dr Josefin Bartholdson, Dr Cecile Crosnier and Dr Madushi Wanaguru). To narrow down the BSG sequence recognised by ch6D9, soluble, biotinylated, BSG domain 1 (d1) and

2 (d2) were expressed recombinantly and tissue culture supernatants were analysed by ELISA for the presence of recombinant proteins. Both BSG d1 and d2 were reactive against the anti-Cd4 monoclonal OX68, confirming recombinant expression (Fig. 4.14A right panel). The binding of ch6D9 to BSG d1 or d2 contained in tissue culture supernatant was then assayed in another round of ELISA. Ch6D9 bound to BSG d1 but not d2 suggesting that ch6D9 epitope is located somewhere within d1 (Fig. 4.14A left panel).

To refine the epitope of ch6D9 on human BSG (*Hs*BSG), a number of constructs encoding for the Cd4-tagged BSG orthologues in gorilla (*Gorilla gorilla*), chimpanzee (*Pan troglodytes*), and marmoset monkey (*Callithrix jacchus*) were employed. The alignment of the ectodomain from all BSG orthologues is shown in Fig. 4.15. Interestingly, chimpanzee ENSPTRP00000017252 (*Pt*BSG) and gorilla ENSGGOP00000022655 (*Gg*BSG) BSG shared a high degree of similarity with *Hs*BSG (about 94%) whereas the similarity between *Callithrix jacchus* (*Cj*BSG) and *Hs*BSG was lower (about 78%). Leucine at position 175 in *Hs*BSG was missing in chimpanzee BSG (*Pt*BSG) but this was probably due to an error arising from incorrect specification of intron-exon boundaries in ENSEMBL genome browser (www.ensembl.org). The identification and analysis of chimpanzee and gorilla BSG was performed by Dr Madushi Wanaguru based on ENSEMBL 2011. Marmoset monkey BSG was cloned from *Cj*cDNA and sequenced by Dr Leyla Bustamante.

All BSG orthologues were recombinantly expressed in a biotinylated form, by transient transfection of the equivalent expression vector into HEK293E cells. The presence of recombinant protein in tissue culture supernatant was confirmed by ELISA (Fig. 4.14B right panel). The binding of ch6D9 to *Pt*BSG, *Gg*BSG and *Cj*BSG was examined in a second ELISA assay. Ch6D9 bound *Pt*BSG to levels similar to *Hs*BSG (Fig. 4.14B left panel). This was expected because *Hs*BSG and *Pt*BSG are identical in d1 (Fig. 4.15). Ch6D9 was not reactive against *Cj*BSG (Fig. 4.14B left panel). Intriguingly, ch6D9 demonstrated reduced binding to *Gg*BSG in comparison to *Hs*BSG suggesting that certain amino acids that differ between *Hs*BSG and *Gg*BSG are likely to be important for ch6D9 binding to BSG. To further investigate the differential binding to *Gg*BSG, a number of *Hs*BSG mutants (H1-H6) were utilized (provided by Dr Madushi Wanaguru). In these constructs, five residues in *Hs*BSG were singly mutated to those found in *Gg*BSG at

A.

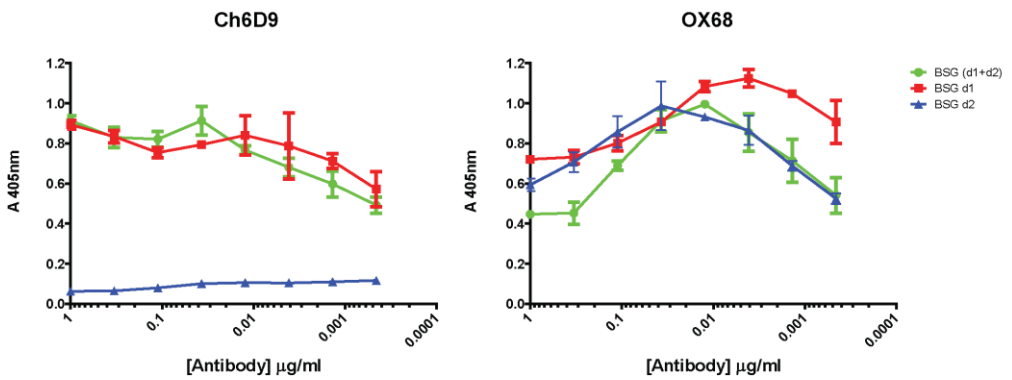

B.

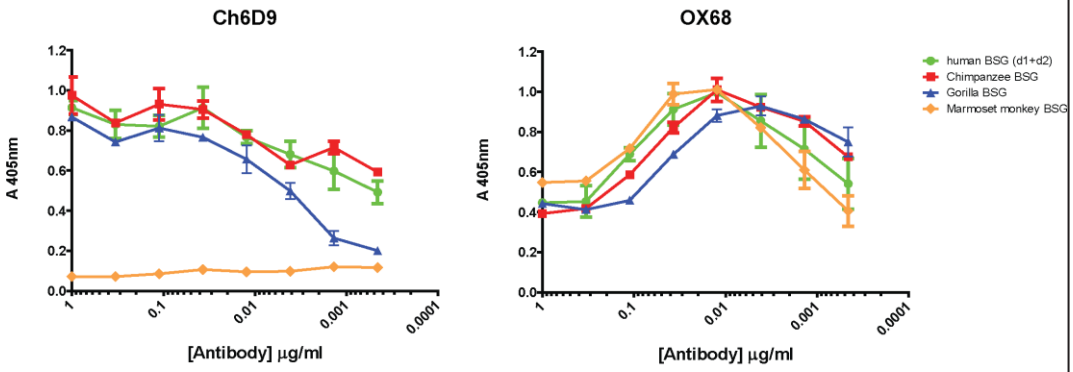

C.

Site directed mutant	Mutation	Location
H1	F27 L	Domain 1
H2	D32 E	
H3	K75 E	
H4	Q100 K	
H5	Insertion H at 103	
H6	S113 L	Domain 2

D.

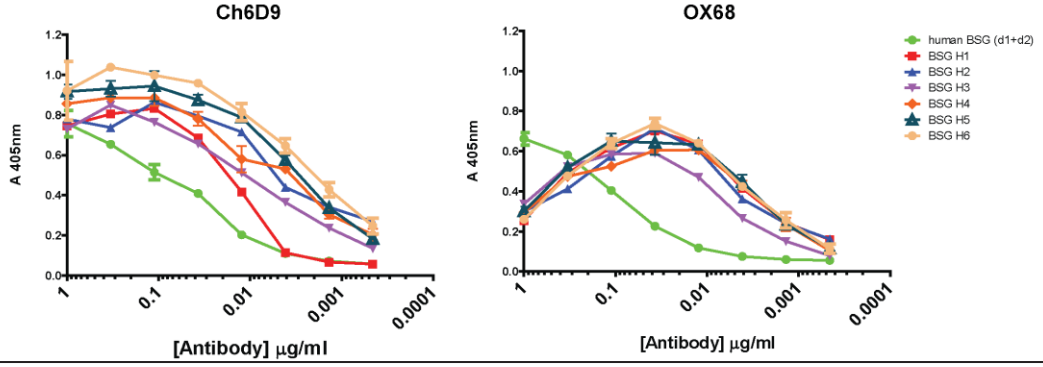

Figure 4.14 Epitope mapping of ch6D9 on BSG.

A. Ch6D9 bound to HsBSG domain 1, as demonstrated by ELISA.

B. Ch6D9 demonstrated binding to Gorilla and Chimpanzee BSG orthologues but not to the marmoset monkey one, as shown by ELISA.

C. Site-directed mutants of *Hs*BSG. Five amino acid residues in *Hs*BSG were mutated to those found in *Gg*BSG at the same position. A Histidine residue was also inserted in *Hs*BSG at position 103, as found in *Gg*BSG (constructs made by Dr Madusi Wanaguru).

D. Ch6D9 recognises BSG H1 mutant with slightly altered affinity, as assessed by ELISA.

The anti-Cd4 antibody OX68 was used to normalise the amounts of BSG proteins. For all ELISAs, the appropriate BSG species/variant from tissue culture supernatant, was immobilised on a streptavidin-coated plate. A dilution series of purified ch6D9 or OX68 was used as primary antibody and an anti-hIgG or anti-mIgG conjugated with alkaline phosphatase as secondary. Abbreviations: d1, BSG domain 1; d2, BSG domain 2. Data in *A*, *B* and *D* are shown as mean ± standard error; n=3.

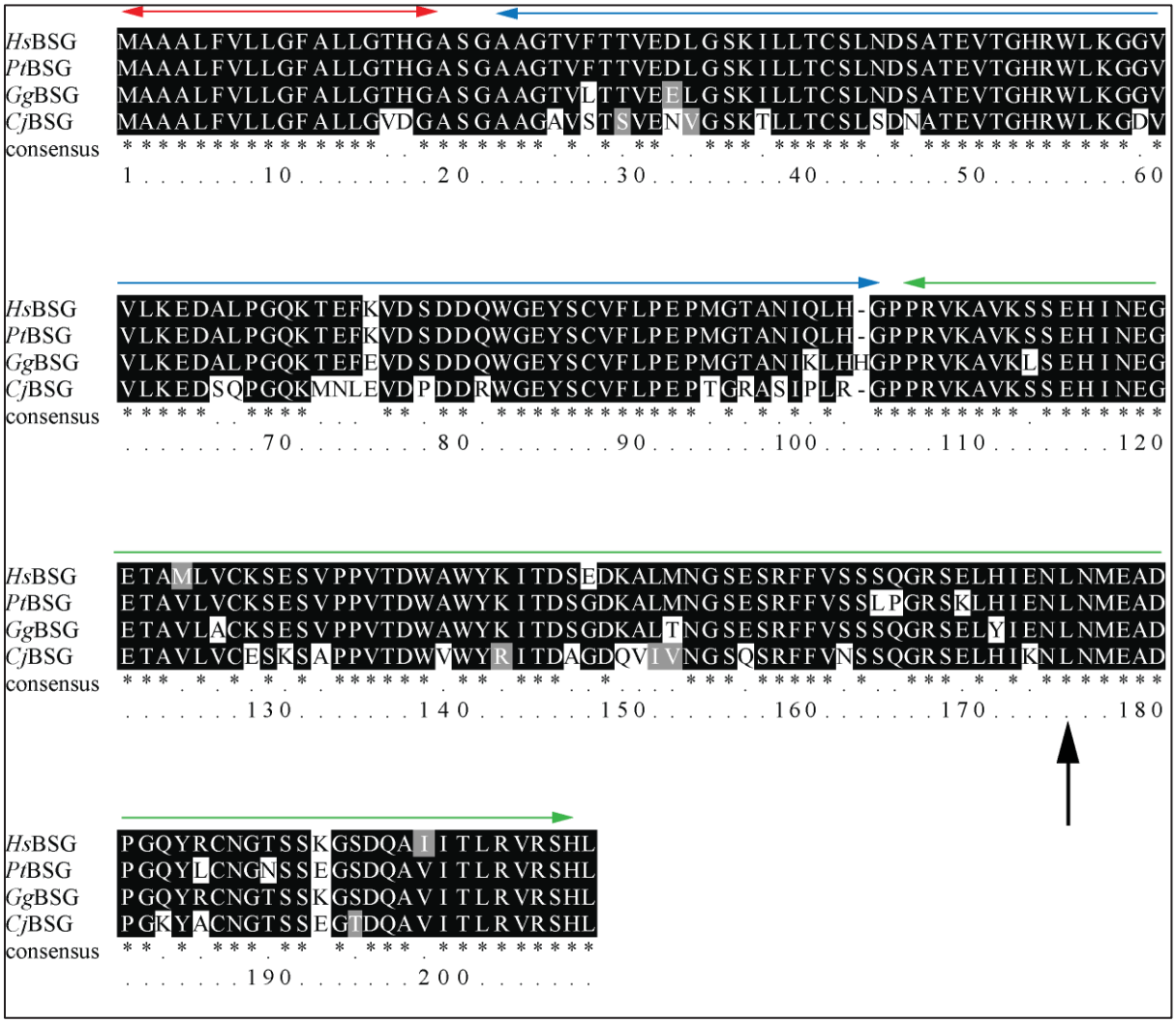

Figure 4.15 Chimpanzee (*Pan troglodytes)* gorilla (*Gorilla gorilla)* and marmoset *(Callithrix jacchus)* orthologues of human (*Homo sapiens*) BSG.

Alignment of the full-length ectodomains of BSG orthologues containing two immunoglobulin-like domains, from human (*Hs*BSG, ENSP00000343809, aa 1-206), chimpanzee (*Pt*BSG, ENSPTRP00000017252, aa 1-206) gorilla (*Gg*BSG, ENSGGOP00000022655, aa 1-207), and marmoset monkey (*Cj*BSG, aa 1-206). Conserved residues are shaded in black and semi-conserved residues in grey. The numbering indicated is for *Gg*BSG. The black arrow marks Leu-175, which is missing from the original *Pt*BSG sequence from Ensembl. The sequences were aligned using ClustalW2 software (Larkin *et al.*, 2007). The signal peptide (aa 1-18), IgSF domain 1 (aa 22-104) and IgSF domain 2 (aa 105-206) (Schlegel *et al.*, 2009) are marked with red, blue and green arrows, respectively. The protein sequences of the predicted BSG orthologues from *P. troglodytes* and *G. gorilla*, were retrieved and analysed from the Ensembl genome browser (Flicek *et al.*, 2011) by Dr Madushi Wanaguru. *Cj*BSG nucleotide sequence was amplified from *Cj*cDNA and sequenced by Dr Leyla Bustamante.

the equivalent positions (Fig. 4.14C). Four of these residues are located in domain 1 and the fifth in domain 2. A Histidine residue was also inserted into the *Hs*BSG sequence at position 103, as found in *Gg*BSG. All six biotinylated *Hs*BSG variants were recombinantly expressed, and the amount of biotinylated protein in each of the preparations was normalised against each other by ELISA (Fig. 4.14D right panel). An ELISA assay was also employed to assess the binding of ch6D9 to the six *Hs*BSG mutants. The binding of ch6D9 to mutants H2-H6 was almost indistinguishable (Fig. 4.14D left panel) between each other. Nevertheless, ch6D9 showed reduced binding to H1 (Fig. 4.14D left panel), suggesting that the phenylalanine at position 27 is likely implicated in the binding of ch6D9 to *Hs*BSG.

4.3.11.3 Biophysical characterisation of mouse and chimeric 6D9

Mouse and chimeric 6D9 were assed for their affinity for BSG by SPR. For this purpose hexa-histidine tagged BSG was purified from tissue culture supernatant by affinity chromatography on a nickel column followed by gel filtration (Fig 4.16A). The protein eluted from the gel filtration column as a monodisperse peak (Fig. 4.16 A). The expected elution volume for BSG monomer was 34.6ml, corresponding to an estimated size of 56.3kDa. Peak fractions containing monomeric protein were pooled and analysed by denaturing SDS-PAGE to confirm presence of BSG at the expected size (Fig 4.16B).

For kinetic analysis, protein G purified mouse (Fig. 4.11A) and chimeric 6D9 (Fig. 4.13A) were *in vitro* biotinylated and captured on the surface of a sensor chip. A dilution series of gel filtrated BSG was injected over the immobilised antibodies and reference substracted sensorgrams were derived. The k_a and k_d values were estimated by globally fitting a 1:1 binding model to the reference subtracted sensorgrams (Fig. 4.16C). Ch6D9 exhibited almost indistinguishable affinity for BSG, in comparison to m6D9 parental antibody (Fig. 4.16D) suggesting that chimerisation did not affect ch6D9 affinity for BSG. The K_D of both chimeric and mouse 6D9 is in the nM range, which is typical for antibody-antigen interactions.

4.3.12 Development and characterisation of a two chimeric anti-RH5 monoclonal antibodies

Dr Simon Draper's group (Jenner Institute, University of Oxford) developed a panel of anti-RH5 monoclonal antibodies, two of which, (2AC7 and 9AD4),

A.

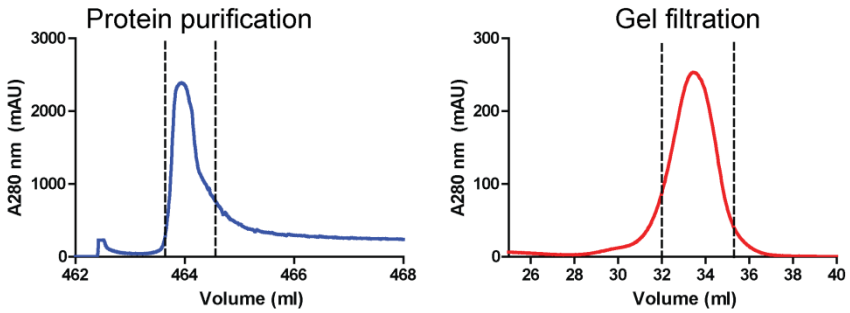

B.

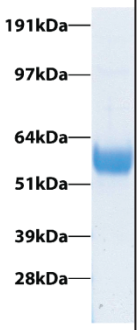

C.

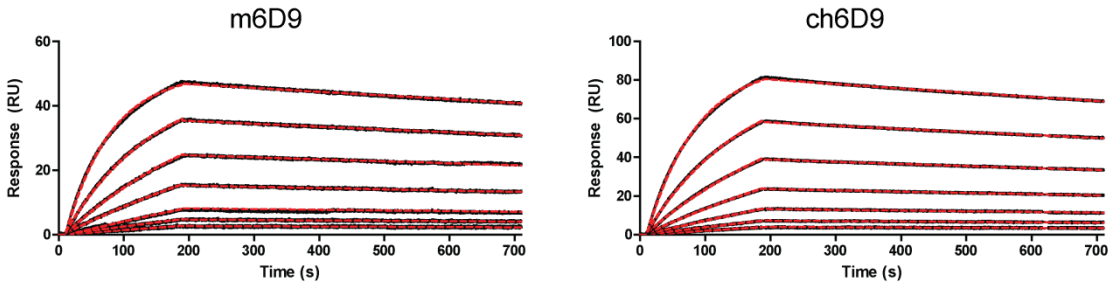

D.

Antibody	k_a ($M^{-1}s^{-1}$)	k_d (s^{-1})	K_D (M)	Chi^2 (RU^2)
m6D9	$(7.02 \pm 0.01)\times10^{4}$	$(2.600 \pm 0.003)\times10^{-4}$	3.767×10^{-9}	0.0672
ch6D9	$(6.27 \pm 0.02)\times10^{4}$	$(2.900 \pm 0.006)\times10^{-4}$	4.742×10^{-9}	0.0672

Figure 4.16 Biophysical analysis of mouse and chimeric 6D9 using SPR.

A. BSG-BLH was affinity purified from tissue culture supernatant, on a nickel column (left), followed by gel filtration (right) to separate monomeric BSG from other forms. The eluate in each of the experiments was monitored at 280 nm in real-time and the peak fractions containing protein (between dashed lines) were pooled. The expected gel filtration elution volume was 34.6ml.

B. Denaturing SDS-PAGE analysis of gel filtrated BSG. The protein was visualised using Coomassie brilliant blue. The expected band size was 56.3kDa.

C. Reference-subtracted sensorgrams (black lines) from the injection of a 2-fold dilution series of BSG (200 - 3.12nM), over the immobilised *in vitro* biotinylated mouse or chimeric 6D9 (ligands). The analyte was injected at a flow rate of 100 µl/min, with a contact time of 180s and a dissociation time of 530s. For the calculation of the association (k_a) and dissociation (k_d) rate constants, a simple Langmuir 1:1 binding model (red dashed lines) was globally fitted to the data. The biotinylated antibodies were immobilised on the chip surface at about 700RU. A mIgG2a or a hIgG1 were used as references.

D. Tables with the kinetic parameters estimated for the binding of mouse or chimeric 6D9 to BSG. For each model, the fit to the experimental data is indicated as the Chi^2 value. The calculated values for the k_a and k_d are indicated with the standard error. K_D was estimated from the equitation $\frac{kd}{ka}$.

demonstrated high efficacy in blocking erythrocyte invasion (Douglas *et al.*, 2013). In order to assess their putative therapeutic potential, I attempted to chimerise them and compare their efficacy with ch6D9. For this purpose, 2AC7 and 9AD4 hybridoma lines were grown in culture, and antibody variable heavy and light chains were amplified and sequenced as described in section 4.3.4 (Fig. 4.17A). Based on the sequencing results, primers were designed for the amplification of 2AC7 and 9AD4 variable regions from TOPO vector (Fig. 4.17B). In parallel, ch6D9 variable heavy or light chain sequences were deleted from the equivalent expression vector by inverted PCR, leaving behind a linear vector carrying the associated signal peptide and constant region, but lacking ch6D9 variable regions (Fig 4.17B). Chimeric 2AC7 and 9AD4 encoding vectors (ch2AC7 and ch9AD4) were generated by blunt-end ligation of 2AC7 and 9AD4 amplicons in between the constant region and signal peptide of the linear vectors (Fig 4.17B).

For recombinant antibody expression, ch2AC7 and ch9AD4 heavy and light chain encoding vectors were co-transfected in HEK293F cells. Tissue culture supernatants were analysed by ELISA for the presence of anti-RH5 antibodies. Both tissue culture supernatants were immunoreactive against RH5, confirming recombinant expression of ch2AC7 and ch9AD4 (Fig 4.17C). To test whether ch2AC7 and ch9AD4 retained their efficacy in blocking erythrocyte invasion, chimeric and mouse 2AC7 and 9AD4 were affinity purified on protein G column (Fig 4.17D), and assayed in *P. falciparum* growth inhibition assay. Ch2AC7 and ch9AD4 prevented erythrocyte invasion at levels comparable to the original mouse antibodies, establishing that chimerisation did not significantly alter their efficacy in inhibiting erythrocyte invasion.

To test whether ch2AC7 and ch9AD4 have retained their affinity for RH5, their binding kinetic parameters were estimated by using SPR. Histidine tagged RH5 was recombinantly expressed and purified by affinity chromatography on nickel column followed by gel filtration (Fig 4.18A). The expected elution volume for full length RH5 monomer was 33.8ml, corresponding to an estimated size of 88kDa (Fig 4.18A). Denaturing SDS-PAGE analysis of the gel filtration peak fraction confirmed the presence of RH5 at the expected size (Fig 4.18B).

For the SPR experiment, purified mouse and chimeric 2AC7 and 9AD4 were *in vitro* biotinylated and immobilised on a sensor chip before a dilution series of RH5

A.

Antibody	Variable region	FR1	CDR1	FR2	CDR2	FR3	CDR3	FR4
2AC7	Heavy	EVKLVESGGGLVQPGGSRKLSCAAS	GFTLSDYG	MAWVRQAPGKGPEWVAF	ISNLAY	SIYYADTVTGRFTISRENDKNTLYLEMNNLRSEDTSMYYC	ARAIFDYDGYWYFDV	WGAGATVTVSS
	Light	DIVLTQSPTSLAVSLGQRATISCRAS	ESVEYYGTSL	IHWFQQKPGQPPKLLIY	AAS	NVESGVPARFSGSGSGTDFSLNIHPVEEDDIAMYFC	QQSKNIPWT	FGGGTKLEIK
9AD4	Heavy	EVKLVESGGGVVQPGGSRKLSCAAS	GFTFSDYG	MAWVRQAPGKGPEWVTF	ISNMAY	SIYYADTVTGRFTISRENAKNTLHLEMSSLRSEDTAMYYC	TRAIFDYAGYWYFDV	WGAGTTVTVSS
	Light	DIVLTQSPASLAVSLGQRATISCRAS	ESVEYYGTSL	MQWFQQKPGQPPRLLIH	GAS	NVQSGVPARFSGSGSGTDFSLNIHPVEEDDFAMYFC	QQSTKVPWT	FGGGTKLEIK

B.

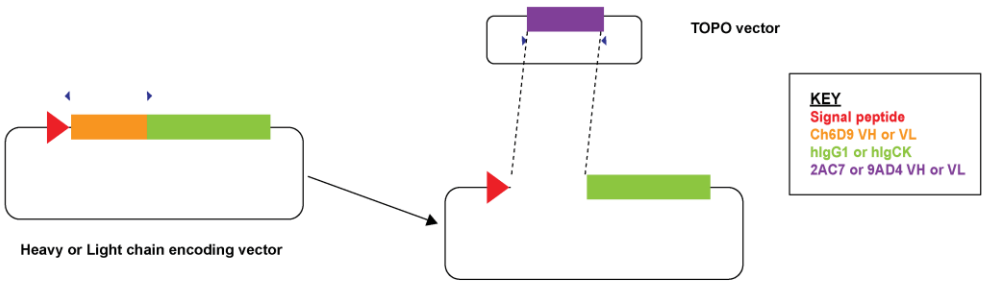

C.

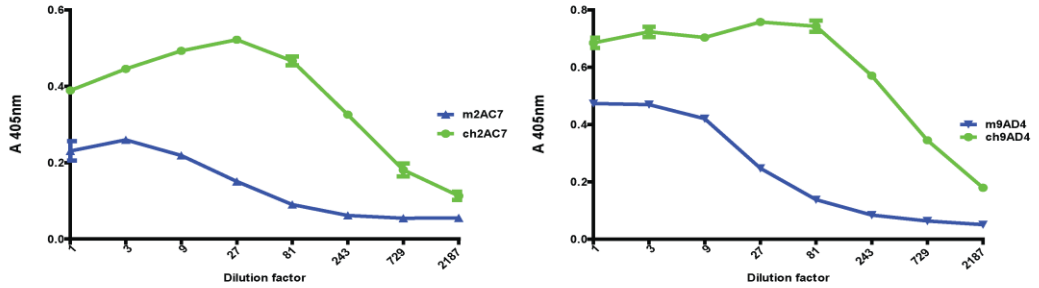

D.

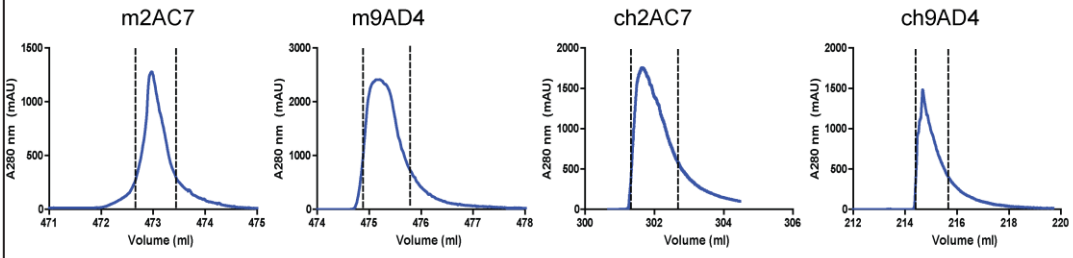

E.

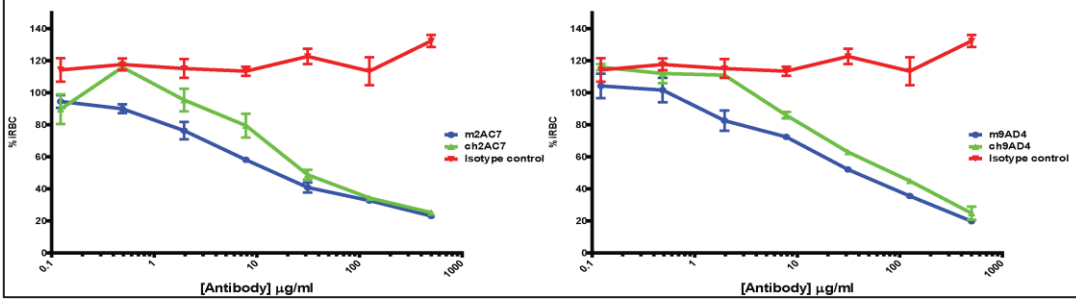

Figure 4.17 Development and characterisation of ch2AC7 and ch9AD4, two chimeric anti-RH5 monoclonal antibodies

A. Sequence analysis of mouse 2AC7 and 9AD4 variable regions. The table shows the amino acid sequence of mouse 2AC7 and 9AD4 rearranged variable heavy (VH) and light (VL) chains as derived from sequence analysis of the amplified variable region from the respective hybridoma cell line.

B. The approach that was followed for the cloning of 2AC7 and 9AD4 variable regions into the heavy and light chain encoding vectors. Ch6D9 variable heavy (VH) or light (VL) chain sequence was deleted from the equivalent vector by inverted PCR. 2AC7 and 9AD4 variable regions were amplified from TOPO vector and blunt ligated into the relevant linear heavy or light chain encoding vector. Blue arrowheads indicate the position of primers.

C. Ch2AC7 (left) and ch9AD4 (right) anti-RH5 antibodies bound to RH5, in an ELISA assay. RH5-BLH from tissue culture supernatant was immobilised on a streptavidin-coated plate at concentrations sufficient for complete saturation of the available binding surface. A 3-fold dilution series of tissue culture supernatant containing ch2AC7 or ch9AD4 was used as primary antibody and an anti-human IgG conjugated with alkaline phosphatase as secondary. M2AC7 and m9AD4 (at starting concentration 2µg/ml) were used as positive controls.

D. Mouse and chimeric 2AC7 and 9AD4 were affinity purified from tissue culture supernatant on protein G column. The eluate in each experiment was monitored at 280 nm in real-time and the peak fractions containing antibody (between dashed lines) were pooled.

E. Protein G purified ch2AC7 and ch9AD4 block *P.falciparum* erythrocyte invasion in culture**.** A synchnonised parasite culture (schizonts) was incubated overnight with a dilution series of ch2AC7 or ch9AD4 followed by fixing, staining and analysis by flow cytometry. M2AC7 and m9AD4 were used as positive controls and an isotype matched antibody, as negative control. The graph shows the percentage of infected red blood cells (iRBC) as a function of antibody concentration.

Data in *C* and *E* are shown as mean ± standard error; n=3.

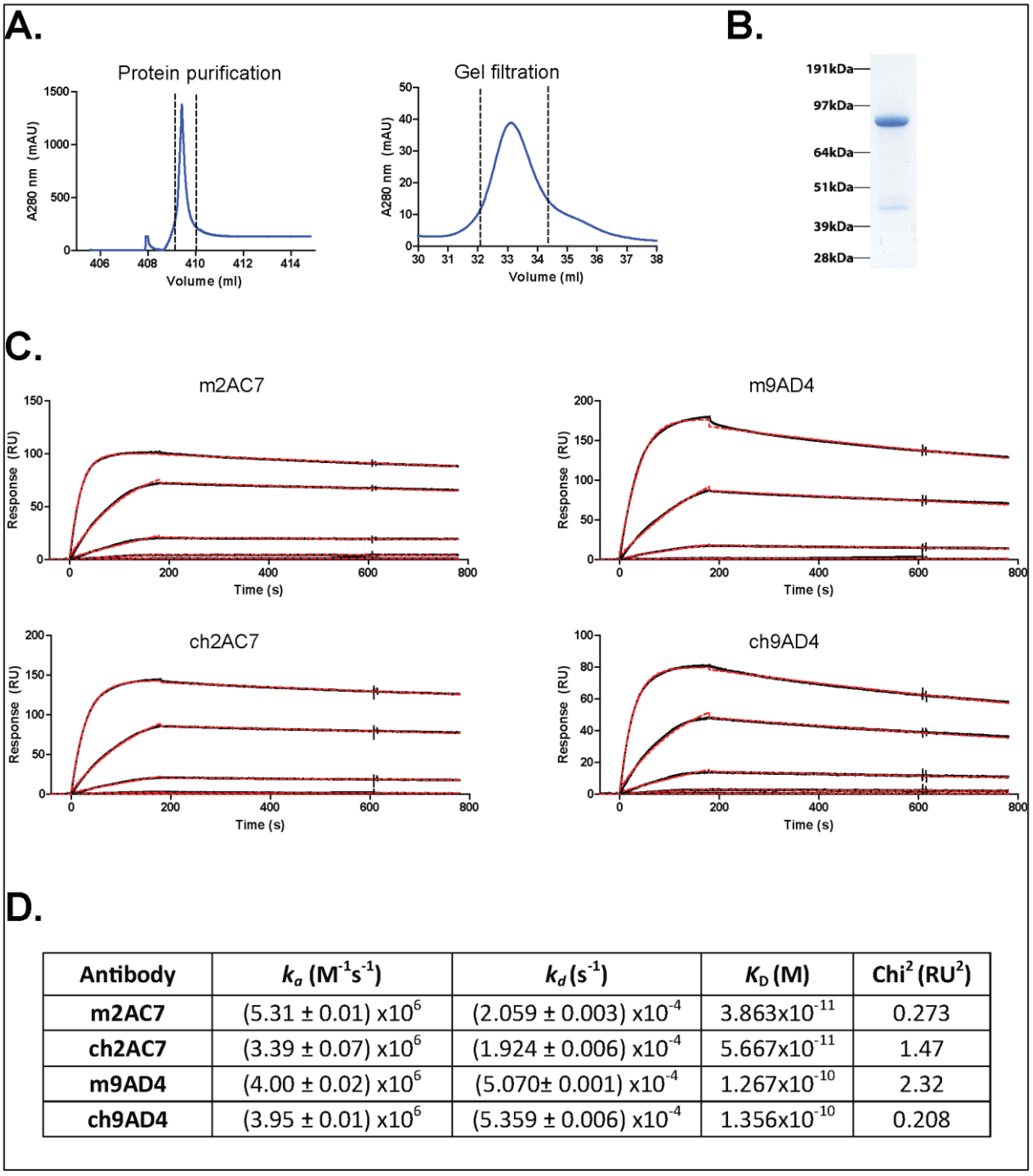

D.

Antibody	k_a ($M^{-1}s^{-1}$)	k_d (s^{-1})	K_D (M)	Chi^2 (RU^2)
m2AC7	(5.31 ± 0.01) x10^6	(2.059 ± 0.003) x10^{-4}	3.863x10^{-11}	0.273
ch2AC7	(3.39 ± 0.07) x10^6	(1.924 ± 0.006) x10^{-4}	5.667x10^{-11}	1.47
m9AD4	(4.00 ± 0.02) x10^6	(5.070± 0.001) x10^{-4}	1.267x10^{-10}	2.32
ch9AD4	(3.95 ± 0.01) x10^6	(5.359 ± 0.006) x10^{-4}	1.356x10^{-10}	0.208

Figure 4.18 Biophysical characterisation of mouse and chimeric 2AC7 and 9AD4 using SPR.

A. Histidine tagged RH5 was affinity purified from tissue culture supernatant, on a nickel column (left), followed by gel filtration (right). The eluate was monitored at 280 nm in real-time and the peak fractions containing protein (between dashed lines) were pooled. The expected gel filtration elution volume was ~33.8ml.

B. Denaturing SDS-PAGE analysis of gel filtrated RH5. The protein was visualised using Coomassie brilliant blue. The expected band size was 88 kDa (including tags).

C. Reference subtracted sensorgrams (black lines) from the injection of a 5-fold dilution series of RH5 (10 - $3.2x10^{-3}$nM), over immobilised *in vitro* biotinylated mouse or chimeric 2AC7 or 9AD4 (ligands). The analyte was injected at a flow rate of 100µl/min, with a contact time of 180s and a dissociation time of 600s. For the calculation of the association (k_a) and dissociation (k_d) rate constants, a simple Langmuir 1:1 binding model (red dashed lines) was globally fitted to the data. The biotinylated antibodies were immobilised on the chip surface at about 550RU. A mIgG2a or a hIgG1 were used as references.

D. Tables with the kinetic parameters estimated for the binding of mouse or chimeric 2AC7 and 9AD4 to RH5. For each model, the fit to the experimental data is indicated as the Chi^2 value. The calculated values for k_a and k_d are indicated with standard error. K_D was estimated from the equitation $\frac{kd}{ka}$.

was injected across the sensor surface. The k_a and k_d values were measured by globally fitting a simple Langmuir binding model to the reference subtracted sensorgrams (Fig 4.18C). Ch2AC7 and ch9AD9 affinity for RH5 was almost identical to their mouse antibody counterparts (Fig 4.18D) suggesting that chimerisation did not alter their affinity for RH5.

4.3.13 Development and characterisation of bi-specific 2AC7-6D9 DVD-Ig

Both humanised anti-BSG (ch6D9) and anti-RH5 (ch2AC7 and ch9AD4) antibodies interfered with erythrocyte invasion in growth inhibition assays. To test whether combining both specificities into a single molecule would have an additive effect in preventing erythrocyte invasion, I sought to combine ch2AC7 and ch6D9 into a single tetravalent immunoglobulin-like molecule which is termed dual-variable-domain immunoglobulin (DVD-Ig; Wu *et al.*, 2007) (Fig. 4.19A).

To develop a 2AC7-6D9 DVD-Ig, 2AC7 variable heavy and light chain sequence was amplified from 2AC7 heavy and light chain encoding vector respectively. Wu and colleagues recommended the development and testing of at least two DVD-Ig versions (short and long), differing in the size of interspace sequence between the two variable domains of different specificity (Wu *et al.*, 2007) (Fig. 4.19A). The size of the linker sequence appears to be important for the flexibility of the variable region, and the appropriate size should be identified by empirical testing. Therefore, two different reverse primers were designed for the amplification of 2AC7 variable heavy or light chain sequence fused to two different sized fragments from hIgG1 or hIgCκ respectively (Fig. 4.19B). In parallel, ch6D9 heavy and light encoding vectors were linearized by inverted PCR. Amplified 2AC7 variable chain sequence fragments (together with the attached sequence encoding for the linker peptide) were ligated in frame to the ch6D9 variable region sequences as shown in Fig. 4.19B.

For recombinant expression, 2AC7-6D9 DVD-Ig heavy and light encoding vectors were co-transfected in HEK293F cells and tissue culture supernatant was collected five days post transfection. Short and long 2AC7-6D9 DVD-Igs were purified from tissue culture supernatant by affinity chromatography on protein G column (Fig. 4.19C). The ability of 2AC7-6D9 DVD-Ig to simultaneously binding to RH5 and BSG was examined by SPR (Fig. 4.19D). *In vitro* biotinylated 2AC7-6D9

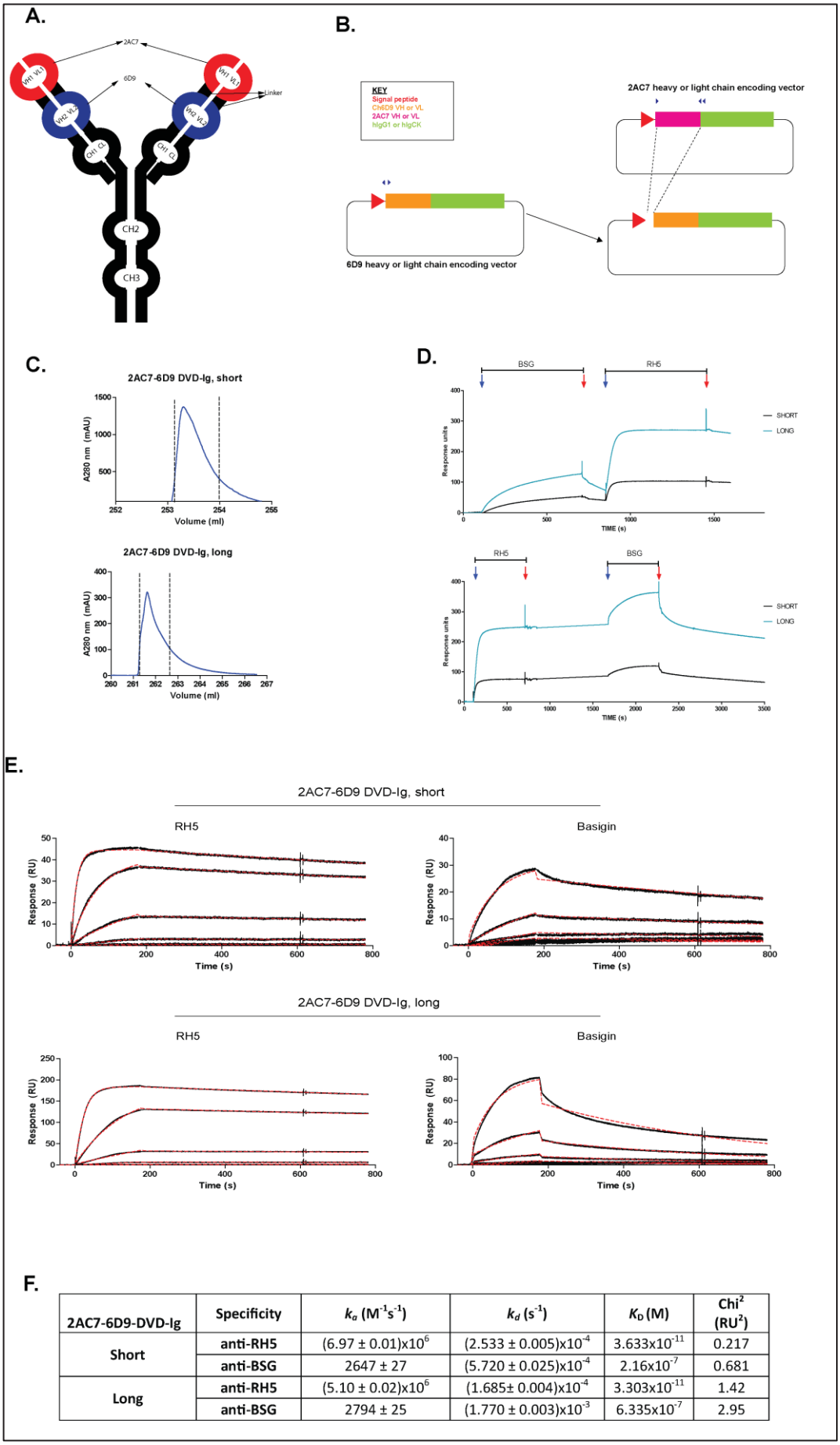

F.

2AC7-6D9-DVD-Ig	Specificity	k_a ($M^{-1}s^{-1}$)	k_d (s^{-1})	K_D (M)	Chi^2 (RU^2)
Short	anti-RH5	$(6.97 \pm 0.01)x10^{6}$	$(2.533 \pm 0.005)x10^{-4}$	$3.633x10^{-11}$	0.217
	anti-BSG	2647 ± 27	$(5.720 \pm 0.025)x10^{-4}$	$2.16x10^{-7}$	0.681
Long	anti-RH5	$(5.10 \pm 0.02)x10^{6}$	$(1.685 \pm 0.004)x10^{-4}$	$3.303x10^{-11}$	1.42
	anti-BSG	2794 ± 25	$(1.770 \pm 0.003)x10^{-3}$	$6.335x10^{-7}$	2.95

Figure 4.19 Generation and biophysical characterisation of a dual specificity 2AC7-6D9 DVD-Ig.

A. Schematic diagram of 2AC7-6D9DVD-Ig protein structure, with two tandem variable domains in each heavy and light chain. Abbreviations: VH1 and VH2, Variable heavy chain 1 and 2; VL1 and VL2, Variable light chain 1 and 2; CH1-3, Constant heavy 1-3; CL, Constant Light.

B. The cloning strategy that was followed for the development of 2AC7-6D9 DVD-Ig. 2AC7 variable heavy (VH) and light (VL) chain sequences together with a small sequence fragment from hIgG1 or hIgCκ respectively, were amplified and cloned into a linearised ch6D9 encoding vector. For the derivation of short and long versions of 2AC7-6D9 DVD-Ig two different reverse primers were used to amplify the 2AC7 variable chain sequences. For more details, see text.

C. 2AC7-6D9 DVD-Igs, short and long, were affinity purified from tissue culture supernatant on protein G column. The eluate in each experiment was monitored at 280 nm in real-time and the peak fractions containing antibody (between dashed lines) were pooled

D. Reference-subtracted sensorgrams from the sequential 600s injection of BSG (5μM) and RH5 (10nM) (without regenerating the surface between injections) over immobilised *in vitro* biotinylated 2AC7-6D9 DVD-Ig short or long version. The sensorgrams suggest that 2AC7-6D9 DVD-Ig can simultaneously bind to RH5 and BSG and this is independent of the order of analyte injection. Blue and red arrows demonstrate the start and end of analyte injection. Bars above the sensograms represent the duration of analyte injection.

E. Reference subtracted sensorgrams (black lines) from the injection of a 5-fold dilution series of RH5 (10 – 6.4x10^{-4}nM) and BSG (5 – 0.32 μM), over the immobilised *in vitro* biotinylated 2AC7-6D9 DVD-Ig short or long. Each time, the analyte was injected at a flow rate of 100μl/min, with a contact time of 180s and a dissociation time of 600s. For the calculation of the association (k_a) and dissociation (k_d) rate constants, a simple Langmuir 1:1 binding model (red dashed lines) was globally fitted to the data. The biotinylated antibodies were immobilised on the chip surface at about 600RU. A hIgG were used as reference.

F. Tables with the kinetic parameters estimated for the binding of 2AC7-6D9 DVD-Ig (short and long) to BSG and RH5. For each model, the goodness of fit to the experimental data is indicated as the Chi^2 value. The calculated values for k_a and k_d are indicated with standard error. K_D was estimated from the equitation $\frac{kd}{ka}$.

DVD-Igs were immobilised on the surface of a sensor chip followed by a sequential injection of BSG and RH5 over the sensor surface. 2AC7-6D9 DVD-Ig was able to bind to both BSG and RH5 at the same time, and the order of binding is not important (Fig. 4.19D). For kinetic analysis, a dilution series of BSG or RH5 was injected across 2AC7-6D9 DVD-Ig captured on the sensor surface. For the derivation of k_a and k_d, a 1:1 binding model was globally fitted to the datasets (Fig. 4.19E). The affinity of both short and long versions of 2AC7-6D9 DVD-Ig for RH5 was almost indistinguishable from ch2AC7 (K_D=~3.5x10^{-11}M). Nevertheless, a fraction of the affinity for BSG was lost in both 2AC7-6D9 DVD-Ig short and long (K_D=~4x10^{-7}M), when compared to ch6D9 (Fig. 4.19F).

The efficacy of 2AC7-6D9 DVD-Ig in preventing erythrocyte invasion was also investigated. A synchronised *P. falciparum* culture at the late trophozoite to early schizont stage was incubated overnight in the presence of a dilution series of purified 2AC7-6D9 DVD-Ig short or long, before analysis of growth inhibition by flow cytometry. The IC_{50} of short 2AC7-6D9 DVD-Ig was significantly lower than ch2AC7 alone, but for the long version the differences were marginal. However, both 2AC7-6D9 DVD-Ig short and long had considerably higher IC_{50} than ch6D9 alone.

These results suggest that ch6D9 is more potent in blocking erythrocyte invasion than 2AC7 or 2AC7-6D9 DVD-Ig, since much lower antibody doses are required for this inhibitory effect (Fig. 4.20).

4.4 Discussion

4.4.1 MEM-6/4 and MEM-M6/8 inhibit the RH5-BSG interaction *in vitro* but not in parasite culture

The central aim this Chapter was the development and characterisation of an anti-BSG humanised or chimeric antibody, as a potential anti-malarial therapeutic. Two anti-BSG mouse monoclonal antibodies, MEM-M6/4 and MEM-M6/8 (Koch *et al.*, 1999), were initially chosen for humanisation. MEM-M6/8 was found to be unable to inhibit erythrocyte invasion in parasite culture and incapable of binding to human erythrocytes (Fig. 4.2). The same antibody however, appeared to block the RH5-BSG interaction *in vitro*, but this was observed only at very high antibody concentrations (Fig. 4.2). I propose two possible explanations for these observations, which are not necessarily mutually exclusive.

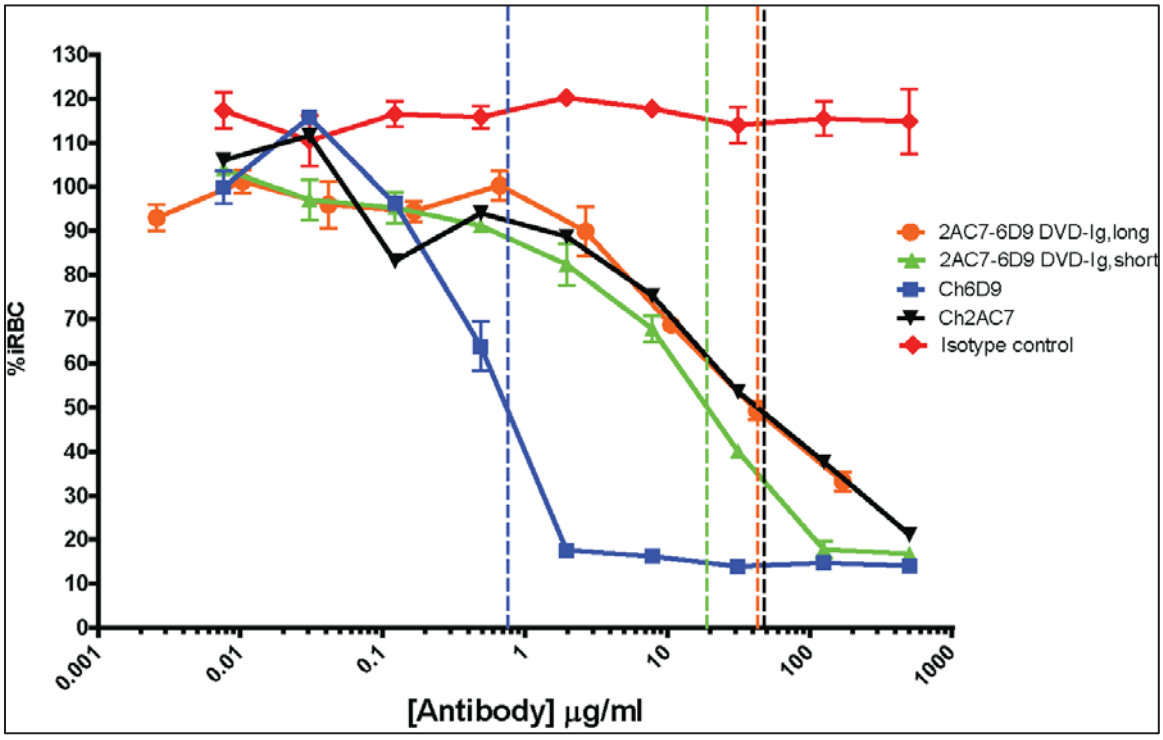

Figure 4.20 ch6D9 is much more potent than ch2AC7 or 2AC7-6D9 DVD-Ig, in blocking erythrocyte invasion. A synchronised parasite culture (schizonts) was incubated overnight with a dilution series of each antibody followed by fixing, staining and analysis by flow cytometry. The graph shows the percentage of infected red blood cells (iRBC) as a function of antibody concentration. An isotype matched antibody was used as negative control. Dashed vertical lines indicate the IC_{50} value for each antibody.

The first explanation is based on the fact that when an antibody is tested for its ability to block an interaction in AVEXIS, two equilibria exist and both need to be taken into account, as shown below.

$$Antibody \quad + \quad Prey \quad \overset{KD1}{\underset{\longleftarrow}{\longrightarrow}} \quad (Antibody - Prey\ complex)$$

$$+$$

$$Bait$$

$$\uparrow\downarrow \text{KD2}$$

$$(Prey\text{-}Bait\ complex)$$

There is one equilibrium between the antibody and prey, and one between the prey and bait. If $K_{D1} << K_{D2}$ the antibody is strongly bound to the prey, and the bait cannot compete for binding. When $K_{D1} \geq K_{D2,}$ the bait becomes a significant competitor to the antibody for binding to the prey and therefore, the interaction between bait and prey is not prevented. In this context, the K_D I calculated for the interaction between MEM-M6/8 and BSG (~1.027 x10^{-6}M), is in the range of the K_D previously reported for the RH5-BSG interaction (~1.2 x10^{-6} M) (Crosnier *et al.*, 2011). Nevertheless, because AVEXIS utilizes pentameric BSG, the overall avidity of the RH5-BSG interaction increases significantly. Therefore, only extraordinary high concentrations of MEM-M6/8 are capable of outcompeting the binding to RH5 and thus inhibiting the interaction. This alone however, does not explain why high concentrations of MEM-M6/8 do not have inhibitory effect in erythrocyte invasion. It is important to mention that there are significant differences in blocking the RH5-BSG interaction *in vitro* by AVEXIS and *ex vivo* in parasite culture. The former system utilizes soluble recombinant proteins of which one of them is a pentamer, whereas the latter is a cell based system where at least one interacting partner (BSG) is membrane embedded. Therefore, parameters which are of little or no importance in first system e.g antibody accessibility, become limiting factors in the second and vice versa.

The second possible explanation – which does not contradict the first one - is based on the fact that antibodies in general are capable of both monovalent and bivalent binding. In the case of clustered antigen, bivalent antibody binding becomes a two state reaction where the engagement of the first antibody binding site brings the second paratope in close vicinity to the target molecule and thereby facilitates its binding. Therefore, the engagement of the first binding site is the limiting factor in this two state reaction.

The soluble pentameric nature of BSG prey used in AVEXIS assay, allows bivalent antibody binding. At (relatively) low concentrations of MEM-M6/8 antibody, monovalent binding occurs, but because the antibody has low affinity for the antigen, it quickly dissociates and cannot be replenished rapidly enough to prevent the binding to bait. Therefore, a significant amount of free BSG still exists, and is capable of binding to RH5 immobilised on the plate. By increasing the concentration of antibody, more monovalent binding exists at a given time point and therefore, bivalent binding is more likely to occur. Bivalently bound MEM-M6/8 results in the formation of stable MEM-M6/8-BSG complexes with extended half-life and thereby the interaction between BSG with RH5 is inhibited.

Bivalent antibody binding requires that two antigen molecules are in close vicinity with each other. Because of the relatively low abundance (~10^5 molecules/cell) of BSG on erythrocyte cell surface (Crosnier *et al.*, 2011; Bartholdson *et al.*, 2013), bivalent binding of MEM-M6/8 to BSG likely did not occur when MEM-M6/8 was used to stain human erythrocytes or to inhibit erythrocyte invasion in *P. falciparum* growth inhibition assay. As a result, monovalently bound MEM-M6/8 quickly dissociated leaving behind “unmasked” BSG which was utilized by the parasite to invade erythrocytes. This hypothesis is supported by previous observations that MEM-M6/8 was unable to stain resting T cells on which BSG is expressed but is of low abundance (Koch *et al.*, 1999). When the same experiment was repeated with PHA activated T cells which have threefold more BSG molecules on their cell surface than resting T cells, MEM-M6/8 binding could be readily detected.

In the same experiments, MEM-M6/4 was shown to be able to bind to both resting and stimulated T cells which is in agreement with my observations that this antibody stains human erythrocytes. The latter result indicates that, in contrast to

MEM-M6/8, monovalent MEM-M6/4 binding is strong enough to survive the washes during staining (Fig. 4.2). Indeed, SPR experiments established that MEM-M6/4 exhibits more than two orders of magnitude higher affinity for BSG than MEM-M6/8 (Fig. 4.9; see below). This however, was not enough for MEM-M6/4 to completely block the RH5-BSG interaction by AVEXIS or to abolish erythrocyte invasion. MEM-M6/4 had a moderate inhibitory effect in parasite growth inhibition assay, which appears to be saturable at about 20% inhibition. Therefore, it is more likely that MEM-M6/4 binds an epitope on BSG which is nearby RH5 binding site, causing a steric effect to the RH5-BSG interaction which in turn reduces invasion efficiency to a certain level (20% inhibition).

4.4.2 The affinity of MEM-6/4 and MEM-M6/8 for BSG is lower than previously reported

Biophysical analysis of MEM-M6/4 and MEM-M6/8 (Fig. 4.9), suggested that the affinities of these antibodies for BSG were three to four orders of magnitude lower than previously reported (Koch *et al.*, 1999). Koch and colleagues used SPR to biophysically analyse MEM-M6/4 and MEM-M6/8. In their experiments they used Fc-fused recombinant BSG as ligand over which they injected the antibodies. To calculate the affinity of MEM-M6/4 and MEM-M6/8 for BSG, it was assumed that there is 1:1 binding, and a predefined Langmuir 1:1 interaction model was fitted to the SPR sensorgrams (Koch *et al.*, 1999). However, there was an important flaw in their experimental design which affected the final results: despite claiming 1:1 stoichiometry between analyte and ligand, it was not taken into account that both analyte and ligand had two binding sites for each other, which significantly increases the overall avidity of the interaction. As a result, the affinity of MEM-M6/4 and MEM-M6/8 for BSG was overestimated.

4.4.3 MEM-6/4 and MEM-M6/8 were successfully humanised

By using the plasmid expression system described in Chapter 3, MEM-M6/4 and MEM-M6/8 were successfully humanised by CDR grafting. HuMEM-M6/4 and huMEM-M6/8 were able to bind BSG *in vitro* by ELISA (Fig. 4.6). HuMEM6/8, similar to the original mouse antibody, had a moderate effect in blocking the RH5-BSG interaction *in vitro*, but could not prevent erythrocyte invasion *ex vivo*. HuMEM-M6/4, unlike its mouse parental antibody, was incapable of staining human erythrocytes

and could not interfere with RH5-BSG interaction *in vitro*, or with erythrocyte invasion in parasite culture, probably due to the decrease in the affinity of huMEM-M6/4 for BSG, in comparison to the mouse parental antibody (Fig. 4.9; see below).

Biophysical analysis of huMEM-M6/4 and huMEM-M6/8 by SPR, suggested that humanisation of these antibodies was accompanied by a decrease in their affinity for BSG. Despite the affinity of huMEM-M6/8 was almost unaltered compared to MEM-M6/8, the affinity of huMEM-M6/4 was reduced by two orders of magnitude in comparison to MEM-M6/4. The decrease in antibody affinities was likely due to incompatibilities between human FRs and murine CDRs. (Lo, 2004; Almagro and Fransson, 2008) Possible ways of restoring the affinity of humanised antibodies for BSG are discussed in Chapter 6.

4.4.4 Development and humanisation of m6D9, a high efficacy anti-BSG antibody

In the current Chapter, I demonstrated that (hu)MEM-M6/4 and (hu)MEM-M6/8 inhibited the RH5-BSG interaction with levels of efficacy below those required for the blockade of erythrocyte invasion in parasite culture. To obtain a more effective anti-BSG monoclonal, a new panel of hybridoma lines secreting anti-BSG antibodies was generated, by directly immunising animals. Initially 11 hybridoma clones were found to secrete antibodies against BSG. However, several hybridomas were later found to have lost their ability to secrete anti-BSG antibodies, probably due to the general genetic instability that accompanies hybridoma clones after fusion (Kromenaker and Srienc, 1994).

The monoclonal antibody m6D9, which was secreted by one of the generated hybridoma clones, demonstrated high efficacy in blocking erythrocyte invasion in parasite culture (Fig. 4.11) and thus, it was selected for humanisation. Humanisation by CDR grafting resulted in the loss of a significant fraction of hu6D9 affinity for BSG (Fig. 4.12). The replacement of two amino acids in huVH which were potentially implicated in the loss of hu6D9 affinity for BSG, did not have the desired result. The loss of hu6D9 affinity is most likely to arise from the incorrect conformation of murine CDRs in the human framework context. Experimental procedures which can potentially restore hu6D9 affinity for BSG are described in Chapter 6.

4.4.5 Ch6D9 is a high affinity anti-BSG chimeric antibody which binds to BSG domain 1

As an alternative to fully humanised hu6D9 a chimeric version of m6D9, ch6D9 was developed. For the creation of ch6D9, intact murine variable heavy and light chains were used and thus, the affinity for BSG was fully retained (Fig. 4.16). Ch6D9 demonstrated high efficacy in inhibiting the RH5-BSG interaction *in vitro*, and in blocking erythrocyte invasion in all four *P. falciparum* strains tested (Fig. 4.13) Therefore, it can be considered for therapeutic purposes.

Epitope mapping experiments demonstrated that ch6D9 binds to BSG domain 1 (Fig. 4.14). To further refine ch6D9 epitope, recombinant *Gg*BSG, *Pt*BSG, and *Cj*BSG were employed. Ch6D9 bound to *Pt*BSG at levels similar to *Hs*BSG. The latter observation was expected because *Pt*BSG and *Hs*BSG are identical in domain 1 (Fig. 4.15) and therefore, *Pt*BSG served as a good internal control. In contrast, no ch6D9 binding to *Cj*BSG was observed. Intriguingly, ch6D9 demonstrated reduced binding to *Gg*BSG in comparison to *Hs*BSG suggesting that certain amino acids that differ between *Hs*BSG and *Gg*BSG are likely important for ch6D9 binding to BSG.

To further refine ch6D9 epitope, a number of *Hs*BSG mutants were used (H1-H6), in which amino acid residues in *Hs*BSG were singly mutated to those found in *Gg*BSG at the same positions (Fig. 4.14). The binding of ch6D9 to H1 BSG mutant considerably decreased in comparison to wild type *Hs*BSG, suggesting that phenylalanine at position 27 is likely part of ch6D9 epitope. These results fit perfectly with previous experiments in our laboratory showing that H1 mutant has 7-fold lower affinity for RH5 than wild type *Hs*BSG (Dr Madushi Wanaguru, unpublished data). The latter observation suggests that phenylalanine at position 27 – which is solvent exposed (Yu *et al.*, 2008) - is probably implicated in RH5-BSG interaction, and in the presence of ch6D9, is likely inaccessible to RH5. However, the possibility that the mutation introduced at position 27 in H1 mutant, simply caused local unfolding which affected both ch6D9 and RH5 binding, cannot be ruled out.

4.4.6 Ch6D9 demonstrates reduced binding to C1q and FcγRIIA

Ch6D9 was very efficient in blocking *P. falciparum* erythrocyte invasion in parasite culture, and it was therefore reasonable to envisage ch6D9 as a putative therapeutic. Nevertheless, the therapeutic value of ch6D9 does not solely rely on its

ability to prevent erythrocyte invasion, but it equally depends on its (in)ability to stimulate ADCC and CDC effector functions which are initiated upon binding of antibody to Fc receptors or recruitment of complement components, respectively. To eliminate antibody effector functions, several mutations were introduced into the Fc region of ch6D9 (Chapter 3)

These mutations were demonstrated to inhibit FcγRIIA and C1q binding to ch6D9. Ideally, the binding of other Fcγ receptors to ch6D9 would have been tested, but attempts to get access to a panel of constructs expressing a range of Fcγ receptors (Shields *et al.*, 2001) were unsuccessful. Nevertheless, the results obtained with FcγRIIA and C1q, suggest that ch6D9 is likely to have reduced ability to trigger ADCC and CDC effector functions.

4.4.7 The potency of ch6D9 in inhibiting erythrocyte invasion is higher than ch2AC7, ch9AD4, or 2AC7-6D9 DVD-Ig

Two chimeric anti-RH5 antibodies, namely ch2AC7 and ch9AD4 were developed. Both antibodies retained their high affinity for RH5 after chimerisation, and were able to inhibit erythrocyte invasion with efficacy similar to the murine parental antibodies (Fig. 4.17). Previous experiments demonstrated that a combination of anti-BSG mAb (TRA-185) and polyclonal rabbit anti-RH5 IgG had an additive effect in blocking erythrocyte invasion in *P. falciparum* parasite culture (Dr Andrew Williams, personal communication). To test whether combining both anti-RH5 and anti-BSG specificities into a single molecule would still have an additive effect in preventing erythrocyte invasion, two versions (short and long) of a bi-specific anti-BSG/RH5 antibody, 2AC7-6D9 DVD-Ig, were developed (Fig. 4.19).

Biophysical analysis of 2AC7-6D9 DVD-Ig demonstrated that both versions were capable of simultaneous binding to RH5 and BSG and the order of binding was not important (Fig. 4.19). Nevertheless, while 2AC7-6D9 DVD-Ig affinity for RH5 was retained in comparison to ch2AC7, the affinity for BSG decreased two orders of the magnitude as compared to ch6D9. It appears that the incorporation of 2AC7 variable heavy and light chain, N-terminally to the respective 6D9 chains, constrained the accessibility of 6D9 variable regions to BSG (DiGiammarino *et al.*, 2012). This is further supported by the biophysical data showing that while the BSG dissociation rate constant (k_d) was only mildly affected (~6-fold and ~2-fold higher in 2AC7-6D9

DVD-Ig short and long respectively, in comparison to ch6D9), the association rate constant (k_a) decreased by a factor of 22 (Fig. 4.19)

Side by side comparison between ch6D9 and ch2AC7 demonstrated that ch6D9 has a considerably higher potency (~50-fold lower IC_{50} than ch2AC7) in inhibiting erythrocyte invasion in parasite culture (Fig. 4.20). Considering that ch2AC7 has two orders of magnitude higher affinity for RH5 than ch6D9 has for BSG, the latter observation cannot be attributed to differences in antibody-antigen affinity between ch2AC7 and ch6D9. The higher potency of ch6D9 is more likely to be due to the binding equilibrium that is reached between ch6D9 and erythrocyte exposed BSG during the invasion assay incubation period. Because of the very transient exposure of RH5 to ch2AC7 during an erythrocyte invasion assay, such equilibrium between ch2AC7 and RH5 can only be achieved by very high concentrations of ch2AC7 (Williams *et al.*, 2012). Similarly, ch6D9 was more potent than 2AC7-6D9 DVD-Ig in preventing erythrocyte invasion. However, as mentioned above, 2AC7-6D9 DVD-Ig has lost a fraction of its affinity for BSG in comparison to ch6D9 and therefore, these data should be interpreted with caution (see Chapter 6).

4.5 Conclusions

In this chapter I described the development of a chimeric anti-BSG antibody, ch6D9, as a potential anti-malarial therapeutic. Ch6D9 retained its high affinity for BSG after chimerisation, and demonstrated high potency in blocking erythrocyte invasion in all parasite lines tested. Furthermore, ch6D9 displayed reduced binding to FcγRIIA and C1q *in vitro*, suggesting that this antibody may have reduced ability to trigger antibody effector functions.

Two chimeric anti-RH5 monoclonal antibodies (ch2AC7 or ch9AD4) and a bi-specific antibody (2AC7-6D9 DVD-Ig) targeting both RH5 and BSG, were also developed. Side by side comparison between ch6D9, ch2AC7 and 2AC7-6D9 DVD-Ig demonstrated that ch6D9 had a considerably lower IC_{50} in blocking erythrocyte invasion in parasite culture, suggesting that the anti-BSG ch6D9 has higher potency in inhibiting erythrocyte invasion, than the other two antibodies tested.